Numerical Methods for Partial Differential Equations

WILEY

RESEARCH ARTICLE OPEN ACCESS

Structure-Preserving Approximation of the Cahn-Hilliard-Biot System

Aaron Brunk[1] | Marvin Fritz[2]

[1]Institute of Mathematics, Johannes Gutenberg University, Mainz, Germany | [2]Computational Methods for PDEs, Johann Radon Institute for Computational and Applied Mathematics, Linz, Austria

Correspondence: Aaron Brunk (abrunk@uni-mainz.de)

Received: 16 July 2024 | **Revised:** 4 October 2024 | **Accepted:** 23 October 2024

Funding: This study was supported by the German Science Foundation (DFG) via TRR 146 (project C3) and SPP2256 Project Number 441153493.

Keywords: Cahn-Hilliard-Biot system | continuous finite elements | convex-concave splitting | structure-preserving approximation | time average

ABSTRACT

In this work, we propose a structure-preserving discretization for the recently studied Cahn-Hilliard-Biot system using conforming finite elements in space and problem-adapted explicit-implicit Euler time integration. We prove that the scheme is thermodynamically consistent, that is, the balance of global phase and global volumetric fluid content and the energy dissipation balance. The existence of discrete solutions is established under suitable growth conditions. Furthermore, it is shown that the algorithm can be realized as a splitting method, that is, decoupling the Cahn-Hilliard subsystem from the poro-elasticity subsystem, while the first one is nonlinear and the second subsystem is linear. The schemes are illustrated by numerical examples and a convergence test.

1 | Introduction

In this paper, we focus on the development and analysis of a structure-preserving discretization scheme for the Cahn-Hilliard-Biot system. This model, originally derived in [1], combines the Cahn-Hilliard equation, which describes phase separation and interfacial dynamics, with mechanical deformation and the Biot equations, which govern fluid flow. The system reads as follows:

$$\partial_t \phi - \operatorname{div}(m(\phi)\nabla\mu) = r(\phi, \mathcal{E}(\mathbf{u}), \theta) \tag{1.1}$$

$$\mu = -\gamma\Delta\phi + \Psi'(\phi) + W_\phi(\phi, \mathcal{E}(\mathbf{u})) - M(\phi)(\theta - \alpha(\phi)\operatorname{div}(\mathbf{u}))\alpha'(\phi)\operatorname{div}(\mathbf{u}) + \frac{M'(\phi)}{2}(\theta - \alpha(\phi)\operatorname{div}(\mathbf{u}))^2 \tag{1.2}$$

$$\operatorname{div}(\boldsymbol{\sigma}) = \mathbf{f} \tag{1.3}$$

$$\boldsymbol{\sigma} = W_{\mathcal{E}}(\phi, \mathcal{E}(\mathbf{u})) + \mathbf{C}_v(\phi)\mathcal{E}(\partial_t \mathbf{u}) - \alpha(\phi)M(\phi)(\theta - \alpha(\phi)\operatorname{div}(\mathbf{u}))\mathbf{I} \tag{1.4}$$

$$\partial_t \theta - \operatorname{div}(\kappa(\phi)\nabla p) = s(\phi, \mathcal{E}(\mathbf{u}), \theta) \tag{1.5}$$

$$p = M(\phi)(\theta - \alpha(\phi)\operatorname{div}(\mathbf{u})) \tag{1.6}$$

The phase-field ϕ represents the two phases -1 and 1, μ the variational derivative of the energy with respect to ϕ, $\mathbf{u}$ the displacement of the elastic body, θ volumetric fluid content, and p the associated pressure. As usual $\mathcal{E}(\mathbf{u}), \mathcal{E}(\partial_t \mathbf{u})$ denote the symmetric part of the gradient of $\mathbf{u}, \partial_t \mathbf{u}$, respectively. The appearing functions will be specified later on. The above system has been derived in [1] as a generalized gradient flow of the energy functional

$$\mathcal{F}(\phi, \mathcal{E}(\mathbf{u}), \theta) = \int_\Omega \frac{\gamma}{2}|\nabla\phi|^2 + \Psi(\phi)\ \mathrm{d}\mathbf{x} + \int_\Omega W(\phi, \mathcal{E}(\mathbf{u}))\ \mathrm{d}\mathbf{x} + \int_\Omega \frac{M(\phi)}{2}(\theta - \alpha(\phi)\operatorname{div}(\mathbf{u}))^2\ \mathrm{d}\mathbf{x} \tag{1.7}$$

where Ω is assumed to be a bounded domain in $\mathbb{R}^d$, $d \in \{2, 3\}$, with sufficiently smooth boundary. We explicitly account for

viscous effects via $\mathbf{C}_v(\phi)\mathcal{E}(\partial_t \mathbf{u})$ as proposed in [2]. The model's ability to account for changes in material properties due to phase transitions makes it particularly relevant for biomedical applications, such as modeling the growth of malignant tumors, which exhibit altered interstitial fluid pressures and changes in the elastic properties of their surrounding matrix [3]. These biophysical changes can significantly impact tumour evolution and response to treatments [4–8]. As done in tumor evolution equations of phase-field type [9–11], we consider $\phi \in [-1, 1]$ as the difference in volume fractions, that is, $\{\phi = 1\}$ represents unmixed tumour tissue, while $\{\phi = -1\}$ represents surrounding healthy tissue.

Previous studies have established the well-posedness of the Cahn-Hilliard-Biot model, proving the existence and uniqueness of weak solutions under various assumptions [2, 12, 13]. The next critical step is to develop numerical methods that preserve the inherent structures and properties of the model, ensuring stability and accuracy in simulations. Structure-preserving discretizations are numerical schemes designed to maintain key properties of the continuous model, such as energy dissipation, phase conservation, and thermodynamic consistency. These properties are crucial for obtaining physically realistic and stable numerical solutions, especially in long-term simulations of complex systems. Several studies have made significant contributions to structure-preserving discretizations with applications to general dissipative problems [14], coupled Cahn-Hilliard equations [15–19], Allen-Cahn equations [20–22], and poro-elasticity [23]. We note that in [24] a fully implicit scheme for the Cahn-Hilliard-Biot system is proposed. However, the focus was on efficient decoupling and not a structure-preserving approximation.

In this work, we propose and analyze a discrete scheme that preserves the gradient flow structure of the Cahn-Hilliard-Biot system. Our approach builds on recent advances in numerical analysis and aims to address the challenges posed by the coupled nonlinearities. We employ a combination of conforming finite element methods and implicit-explicit (IMEX) Euler time integration, tailored to respect the model's thermodynamic framework. By preserving the discrete energy laws and ensuring consistent approximations of the coupled variables, our methods achieve robust performance and accurate representations of the underlying physical processes.

Numerical methods for the related Cahn-Hilliard-Larché equations, which couple the Cahn-Hilliard equation with elasticity, have seen significant advances in recent years. We mention the fully practical finite element approximation showing stability and convergence in [25], the experimental observations in superalloys in [26], the finite difference schemes for the 1D system proving error estimates in [19, 27], the adaptive mesh refinement and multigrid methods for efficient and reliable simulation in [28], the inclusion of stress-driven interface motion in [29], the convergence of a finite element and implicit Euler scheme in [30], the isogeometric analysis in topology optimisation problems in [31], and the posteriori error analysis in [32]. Discretisation based on convex-concave decomposition with alternative minimization can be found in [33]. Also related method for Cahn-Hilliard with finite strain using a staggered approach is given in [34].

The structure of this article is as follows: In Section 2, we introduce the variational formulation and the relevant assumptions of the model. In Section 3, we detail the proposed structure-preserving discretization method and state the main theorem of this work, that is, there is a discrete solution that conserves the global phase, volumetric fluid content and energy-dissipation balances. Section 4 provides a rigorous proof of the proposed theorem. Finally, Section 5 showcases numerical experiments that validate our theoretical findings and demonstrate the practical effectiveness of our methods in simulating tumor growth.

2 | Notation and Variational Formulation

Throughout the text, we use standard notation for function spaces and norms; see, for instance [35]. For ease of notion, we write $\langle \cdot, \cdot \rangle$ for the $L^2(\Omega)$-inner product, $\| \cdot \|_{s,p}$, $s \in \mathbb{R}$, $p \geq 1$, for the norm of the Sobolev space $W^{s,p}(\Omega)$, and shortly $\| \cdot \|_s := \| \cdot \|_{s,2}$.

Using the energy functional $\mathcal{F}$, see (1.7), we can reveal the gradient structure of the system. Indeed, by recognizing μ, p and partly σ as variational derivatives of F, we find:

$$\partial_t \phi - \operatorname{div}(m(\phi)\nabla \mu) = r(\phi, \mathcal{E}(\mathbf{u}), \theta), \qquad \mu = \frac{\delta \mathcal{F}}{\delta \phi} \tag{2.1}$$

$$\operatorname{div}(\boldsymbol{\sigma}) = \frac{\delta \mathcal{F}}{\delta \mathcal{E}(\mathbf{u})} + \operatorname{div}(\mathbf{C}_v(\phi)\mathcal{E}(\partial_t \mathbf{u})) = \mathbf{f} \tag{2.2}$$

$$\partial_t \theta - \operatorname{div}(\kappa(\phi)\nabla p) = s(\phi, \mathcal{E}(\mathbf{u}), \theta), \qquad p = \frac{\delta \mathcal{F}}{\delta \theta} \tag{2.3}$$

We make the following assumptions and choices:

(A0) $\Omega \subset \mathbb{R}^d$, $d \in \{2, 3\}$, is Lipschitz continuous, and we consider the boundary conditions

$$\mathbf{u}|_{\partial\Omega} = \mathbf{0}, \quad \kappa(\phi)\nabla p \cdot \mathbf{n}|_{\partial\Omega} = \nabla \phi \cdot \mathbf{n}|_{\partial\Omega} = m(\phi)\nabla \mu \cdot \mathbf{n}|_{\partial\Omega} = 0$$

(A1) the interface parameter γ is a positive constant;

(A2) the Cahn-Hilliard potential $\Psi \in C^2(\mathbb{R})$ is bounded from below and admits a decomposition into a convex and concave part $\Psi_{\text{vex}}, \Psi_{\text{cav}}$; furthermore, we assume that $|\Psi(x)| \leq c_1|x|^p + c_2$ for $p \leq 6$ and non-negative constants c_1, c_2;

(A3) the elastic energy W is given by $W(x, \mathcal{G}) = (\mathcal{G} - \mathcal{T}(x)) : \mathbf{C}(x) : (\mathcal{G} - \mathcal{T}(x))$ for $x \in \mathbb{R}$, $\mathcal{G} \in \mathbb{R}^{d\times d}$ with symmetric eigenstrain $\mathcal{T} \in C^2(\mathbb{R})$ and symmetric elastic tensor $\mathbf{C} \in C^2(\mathbb{R})$ such that

$$\mathcal{G} : \mathbf{C}(x) : \mathcal{G} \geq c|G|^2$$
$$\mathcal{D} : \mathbf{C}(x) : \mathcal{G} = \mathcal{D} : \mathbf{C}(x)\mathcal{G} = \mathbf{C}(x)\mathcal{D} : \mathcal{G}$$

for any $x \in \mathbb{R}$, $\mathcal{D}, \mathcal{G} \in \mathbb{R}^{d\times d}_{\text{sym}}$; for simplicity, let us assume that $\mathcal{T}(x) = \xi(x - \alpha)\mathbf{I}$ for suitable constants ξ, α; furthermore, we assume that all derivatives of $\mathbf{C}$ are uniformly bounded from above and below.

(A4) the modulus of viscoelasticity $\mathbf{C}_v(\phi)$ fulfills the same assumptions as $\mathbf{C}(\phi)$;

(A5) the diffusion coefficients m and κ are positively bounded from above and below, that is, there exist positive constants $m_0, m_1, \kappa_0, \kappa_1$ such that $m_0 \le m(x) \le m_1$ and $\kappa_0 \le \kappa(x) \le \kappa_1$ for any $x \in \mathbb{R}$;

(A6) the functions M and α are positively bounded from above and below, that is, there exist positive constants $M_0, M_1, \alpha_0, \alpha_1$ such that $M_0 \le M(x) \le M_1$ and $\alpha_0 \le \alpha(x) \le \alpha_1$ for any $x \in \mathbb{R}$; further, the functions are sufficiently regular with bounded derivatives, that is, $|\alpha^{(k)}(x)| \le \alpha_{k+1}$ and $|M^{(k)}(x)| \le M_{k+1}$, $k \in \{1, 2\}$, for any $x \in \mathbb{R}$;

(A7) $\mathbf{f} \in L^2(0, T; H^{-1}(\Omega))$ and the source terms $r, s \in C^1(\mathbb{R} \times \mathbb{R}^{d\times d} \times \mathbb{R})$ are uniformly bounded.

In the following, we will denote by $F(\phi, \mathcal{E}(\mathbf{u}), \theta)$ the density of the energy functional $\mathcal{F}$. We introduce the reduced energy density, that is, the energy density for the poro-elastic subsystem, via

$$\widetilde{W}(\phi, \mathcal{E}(\mathbf{u}), \theta) := W(\phi, \mathcal{E}(\mathbf{u})) + \frac{M(\phi)}{2}(\theta - \alpha(\phi)\mathrm{tr}(\mathcal{E}(\mathbf{u})))^2 \quad (2.4)$$

Note that in view of the above assumptions, we observe that $\widetilde{W}$ is convex in $(\mathcal{E}(\mathbf{u}), \theta)$ for every fixed $\phi \in \mathbb{R}$. Furthermore, we will denote the partial derivatives of the energy density F by $F_\phi, F_{\nabla\phi}, F_{\mathcal{E}(\mathbf{u})}, F_\theta$ and similarly for the reduced energy density $\widetilde{W}$.

We remark that one can also use Dirichlet boundary conditions for p or mixing both sets of conditions by introducing a Dirichlet and a Neumann boundary part, as done in [2]. Furthermore, for the analysis, the term $\mathrm{div}(\mathbf{C}_v\mathcal{E}(\mathbf{u}))$ can also be replaced by $\mathrm{div}(c_v\mathrm{div}(\mathbf{u}))$, see [13] for existence results of such a regularization.

Variational Formulation: The above system can be directly converted into a variational formulation, which reads as follows:

$$\langle \partial_t\phi, \psi\rangle + \langle m(\phi)\nabla\mu, \nabla\psi\rangle = \langle r(\phi, \mathcal{E}(\mathbf{u}), \theta), \psi\rangle \quad (2.5)$$

$$\langle \mu, \xi\rangle = \langle F_{\nabla\phi}(\nabla\phi), \nabla\xi\rangle + \langle F_\phi(\phi, \mathcal{E}(\mathbf{u}), \theta), \xi\rangle \quad (2.6)$$

$$\langle F_{\mathcal{E}(\mathbf{u})}(\phi, \mathcal{E}(\mathbf{u}), \theta) + \mathbf{C}_v(\phi)\mathcal{E}(\partial_t\mathbf{u}), \mathcal{E}(\mathbf{v})\rangle = \langle \mathbf{f}, \mathbf{v}\rangle \quad (2.7)$$

$$\langle \partial_t\theta, \chi\rangle + \langle \kappa(\phi)\nabla p, \nabla\chi\rangle = \langle s(\phi, \mathcal{E}(\mathbf{u}), \theta), \chi\rangle \quad (2.8)$$

$$\langle p, q\rangle = \langle F_\theta(\phi, \mathcal{E}(\mathbf{u}), \theta), q\rangle \quad (2.9)$$

where ψ, ξ, $\mathbf{v}$, χ, and q are suitable test functions. The energy dissipation law of the system can then be obtained by choosing specific test functions.

Lemma 2.1. *Sufficiently regular solutions of the system (2.1–2.3) satisfy the variational formulations (2.5–2.9). Furthermore, the balance of global phase and volumetric fluid content as well as the energy-dissipation balance hold, which are given by*

$$\frac{\mathrm{d}}{\mathrm{d}t}\langle \phi, 1\rangle = \langle r(\phi, \mathcal{E}(\mathbf{u}), \theta), 1\rangle$$
$$\frac{\mathrm{d}}{\mathrm{d}t}\langle \theta, 1\rangle = \langle s(\phi, \mathcal{E}(\mathbf{u}), \theta), 1\rangle$$
$$\frac{\mathrm{d}}{\mathrm{d}t}\mathcal{F}(\phi, \mathcal{E}(\mathbf{u}), \theta) = -\mathcal{D}_\phi(\mu, \partial_t\mathbf{u}, p) + \mathcal{P}_{\phi,\mathcal{E}(\mathbf{u}),\theta}(\mu, \partial_t\mathbf{u}, p)$$

with dissipation rate

$$\mathcal{D}_\phi(\mu, \partial_t\mathbf{u}, p) := \langle m(\phi)\nabla\mu, \nabla\mu\rangle + \langle \mathbf{C}_v(\phi)\mathcal{E}(\partial_t\mathbf{u}), \mathcal{E}(\partial_t\mathbf{u})\rangle + \langle \kappa(\phi)\nabla p, \nabla p\rangle$$

and source rate

$$\mathcal{P}_{\phi,\mathcal{E}(\mathbf{u}),\theta}(\mu, \partial_t\mathbf{u}, p) := \langle r(\phi, \mathcal{E}(\mathbf{u}), \theta), \mu\rangle + \langle \mathbf{f}, \partial_t\mathbf{u}\rangle + \langle s(\phi, \mathcal{E}(\mathbf{u}), \theta), p\rangle$$

Proof. First, we note that the variational form can be deduced by multiplying the system (2.1–2.3) with sufficiently regular test functions and applying the usual integration by parts. Regarding the balance of the phase and volumetric fluid content, we insert the test functions $\psi = 1$ and $\chi = 1$ into the variational forms (2.5) and (2.8), respectively. In fact, this procedure immediately yields the desired results. For the energy-dissipation balance, we compute the total derivative of the energy functional $\mathcal{F}$, see (1.7),

$$\frac{\mathrm{d}}{\mathrm{d}t}\mathcal{F}(\phi, \mathcal{E}(\mathbf{u}), \theta) = \left\langle \frac{\partial F}{\partial\nabla\phi}, \nabla\partial_t\phi\right\rangle + \left\langle \frac{\partial F}{\partial\phi}, \partial_t\phi\right\rangle + \left\langle \frac{\partial F}{\partial\mathcal{E}(\mathbf{u})}, \mathcal{E}(\partial_t\mathbf{u})\right\rangle + \left\langle \frac{\partial F}{\partial\theta}, \partial_t\theta\right\rangle$$

Taking the test functions $\xi = \partial_t\phi$ and $q = \partial_t\theta$ in the variational forms (2.6) and (2.9), respectively, further yields

$$= \langle \mu, \partial_t\phi\rangle + \langle F_{\mathcal{E}(\mathbf{u})}, \mathcal{E}(\partial_t\mathbf{u})\rangle + \langle p, \partial_t\theta\rangle$$

Using the variational formulations (2.5), (2.7) and (2.8) with the test functions $\psi = \mu$, $\mathbf{v} = \partial_t\mathbf{u}$, and $\chi = p$ finally yields

$$= -\langle m(\phi)\nabla\mu, \nabla\mu\rangle - \langle \mathbf{C}_v(\phi)\mathcal{E}(\partial_t\mathbf{u}), \mathcal{E}(\partial_t\mathbf{u})\rangle - \langle \kappa(\phi)\nabla p, \nabla p\rangle + \langle r(\phi, \mathcal{E}(\mathbf{u}), \theta), \mu\rangle + \langle \mathbf{f}, \partial_t\mathbf{u}\rangle + \langle s(\phi, \mathcal{E}(\mathbf{u}), \theta), p\rangle$$

which proves the desired energy-dissipation balance. □

3 | Structure-Preserving Discretisation

As a preparatory step, we introduce the relevant notation and assumptions regarding the discretization strategy for the Cahn-Hilliard-Biot system.

For spatial discretization, we require that $\mathcal{T}_h$ is a geometrically conforming partition of Ω into simplices. We denote the space of continuous, piecewise linear functions over $\mathcal{T}_h$ and the space with zero Dirichlet data by

$$\mathcal{V}_h := \{v \in H^1(\Omega) \cap C^0(\overline{\Omega}) : v|_K \in P_1(K) \quad \forall K \in \mathcal{T}_h\}$$
$$\mathcal{X}_h := \{v \in \mathcal{V}_h : v|_{\partial\Omega} = 0\}$$

respectively. We divide the time interval $[0, T]$ into uniform steps with step size $\tau > 0$ and introduce

$$\mathcal{I}_\tau := \{0 = t^0, t^1 = \tau, \ldots, t^{n_T} = T\}$$

where $n_T = \frac{T}{\tau}$ is the absolute number of time steps. We denote by $\Pi^1_c(\mathcal{I}_\tau; X)$ and $\Pi^0(\mathcal{I}_\tau; X)$ the spaces of continuous piecewise

linear and piecewise constant functions on $\mathcal{I}_\tau$ with values in the space X, respectively. By g^{n+1} and g^n we denote the evaluation/approximation of a function g in $\Pi_c^1(\mathcal{I}_\tau)$ or $\Pi^0(\mathcal{I}_\tau)$ at $t = \{t^{n+1}, t^n\}$, respectively, and write $I_n = (t^n, t^{n+1})$. We introduce the following operators and abbreviations:

- The time difference and the discrete time derivative, respectively, are denoted by

$$d^{n+1}g := g^{n+1} - g^n, \qquad d_\tau^{n+1}g := \frac{g^{n+1} - g^n}{\tau}$$

- The time average of a function $g(\rho)$ for $\rho \in \Pi_c^1(\mathcal{I}_\tau)$ is given by

$$g^{av}(\rho) := \frac{1}{\tau}\int_{I_n} g(\rho(s))\ \mathrm{d}s$$

- The convex-concave splitting of the Cahn-Hilliard potential Ψ is denoted by

$$\Psi'(\phi_h^{n+1}, \phi_h^n) := \Psi'_{\mathrm{vex}}(\phi_h^{n+1}) + \Psi'_{\mathrm{cav}}(\phi_h^n)$$

Next, we state the fully discrete scheme of the Cahn-Hilliard-Biot system that we analyze in this work.

Problem 1. Let the initial data $(\phi_{h,0}, \mathbf{u}_{h,0}, \theta_{h,0}) \in \mathcal{V}_h \times \mathcal{X}_h^d \times \mathcal{V}_h$ be given. Find $(\phi_h, \mathbf{u}_h, \theta_h) \in \Pi_c^1(\mathcal{I}_\tau; \mathcal{V}_h \times \mathcal{X}_h^d \times \mathcal{V}_h)$ and $(\mu_h, p_h) \in \Pi^0(\mathcal{I}_\tau; \mathcal{V}_h \times \mathcal{V}_h)$ that satisfy the variational system

$$\langle d_\tau^{n+1}\phi_h, \psi_h\rangle + \langle m(\phi_h^n)\nabla\mu_h^{n+1}, \nabla\psi_h\rangle = \langle r(\phi_h^n, \mathcal{E}(\mathbf{u}_h^{n+1}), \theta_h^{n+1}), \psi_h\rangle \tag{3.1}$$

$$\begin{aligned}\langle \mu_h^{n+1}, \xi_h\rangle - \gamma\langle\nabla\phi_h^{n+1}, \nabla\xi_h\rangle - \langle\Psi'(\phi_h^{n+1}, \phi_h^n)\\ + \widetilde{W}_\phi^{av}(\phi_h, \mathcal{E}(\mathbf{u}_h^{n+1}), \theta_h^{n+1}), \xi_h\rangle = 0\end{aligned} \tag{3.2}$$

$$\begin{aligned}&\langle \mathbf{C}_v(\phi_h^n)\mathcal{E}(d_\tau^{n+1}\mathbf{u}_h), \mathcal{E}(\mathbf{v}_h)\rangle\\ &\quad + \langle \widetilde{W}_{\mathcal{E}(\mathbf{u})}(\phi_h^n, \mathcal{E}(\mathbf{u}_h^{n+1}), \theta_h^{n+1}), \mathcal{E}(\mathbf{v}_h)\rangle = \langle \mathbf{f}^{n+1}, \mathbf{v}_h\rangle\end{aligned} \tag{3.3}$$

$$\langle d_\tau^{n+1}\theta_h, \chi_h\rangle + \langle \kappa(\phi_h^n)\nabla p_h^{n+1}, \nabla\chi_h\rangle = \langle s(\phi_h^n, \mathcal{E}(\mathbf{u}_h^n), \theta_h^n), \chi_h\rangle \tag{3.4}$$

$$\langle p_h^{n+1}, q_h\rangle - \langle \widetilde{W}_\theta(\phi_h^n, \mathcal{E}(\mathbf{u}_h^{n+1}), \theta_h^{n+1}), q_h\rangle = 0 \tag{3.5}$$

for every $(\psi_h, \xi_h, \mathbf{v}_h, \chi_h, q_h) \in \mathcal{V}_h \times \mathcal{V}_h \times \mathcal{X}_h^d \times \mathcal{V}_h \times \mathcal{V}_h$ and every $0 \le n \le n_T - 1$.

From a naive point of view, one would try to use convex-concave decomposition for all terms in the energy related to ϕ. In principle, this might be possible, but since several terms change, this is inconvenient. To resolve this problem, we use the time average technique, which basically amounts to integrating the ϕ dependent coefficients exactly in time. From a computational point of view, we employ a high-order quadrature rule; hence, it is exact for polynomial nonlinearities. This introduces no significant overhead since the evaluation at the quadrature nodes is given by a linear combination of the two available time-steps of ϕ. The properties of this scheme are condensed into the following theorem.

Theorem 1. *Let (A0)–(A7) hold. Furthermore, let $\tau \le C_0$ for $C_0 > 0$ depend solely on the parameters and external forces. Then, for any $(\phi_{h,0}, \mathbf{u}_{h,0}, \theta_{h,0}) \in \mathcal{V}_h \times \mathcal{X}_h^d \times \mathcal{V}_h$, Problem 1 admits at least one solution $(\phi_h, \mu_h, \mathbf{u}_h, \theta_h, p_h)$. Moreover, any such solution conserves the global phase and volumetric fluid content balances and the energy-dissipation balance, that is, it holds*

$$\langle \phi_h^n, 1\rangle = \langle \phi_h^m, 1\rangle + \tau\sum_{k=m}^{n-1}\langle r(\phi_h^k, \mathcal{E}(\mathbf{u}_h^{k+1}), \theta_h^{k+1}), 1\rangle \tag{3.6}$$

$$\langle \theta_h^n, 1\rangle = \langle \theta_h^m, 1\rangle + \tau\sum_{k=m}^{n-1}\langle s(\phi_h^k, \mathcal{E}(\mathbf{u}_h^k), \theta_h^k), 1\rangle \tag{3.7}$$

$$\begin{aligned}&\mathcal{F}(\phi_h, \mathcal{E}(\mathbf{u}_h), \theta_h)\big|_{t^m}^{t^n} + \int_{t^m}^{t^n}\mathcal{D}^*(\mu_h, \partial_t\mathbf{u}_h, p_h)\ \mathrm{d}s\\ &\quad \le \int_{t^m}^{t^n}\mathcal{P}^*(\mu_h, \partial_t\mathbf{u}_h, p_h)\ \mathrm{d}s\end{aligned} \tag{3.8}$$

The discrete dissipation and source rate in the above equation are given by

$$\int_{t^m}^{t^n}\mathcal{D}^*(\mu_h, \partial_t\mathbf{u}_h, p_h)\,\mathrm{d}s := \tau\sum_{k=m}^{n-1}\mathcal{D}_{\phi_h^k}(\mu_h^{k+1}, d_\tau^{k+1}\mathbf{u}_h, p_h^{k+1})$$

$$\begin{aligned}\int_{t^m}^{t^n}\mathcal{P}^*(\mu_h, \partial_t\mathbf{u}_h, p_h)\,\mathrm{d}s &:= \tau\sum_{k=m}^{n-1}\langle r(\phi_h^k, \mathcal{E}(\mathbf{u}_h^{k+1}), \theta_h^{k+1}), \mu_h^{k+1}\rangle\\ &\quad + \langle \mathbf{f}^{k+1}, d_\tau^{k+1}\mathbf{u}_h\rangle + \langle s(\phi_h^k, \mathcal{E}(\mathbf{u}_h^k), \theta_h^k), p_h^{k+1}\rangle\end{aligned}$$

For quasi-uniform meshes and under a CFL-type condition $2C_1\tau \le h^{2d}$, the solution is unique. Here, $C_1 > 0$ depends on the parameters, the initial data, and the external forces.

We emphasize that the preservation of global phase, global volumetric fluid content, and energy-dissipation balance holds for any $h, \tau > 0$ given that a solution exists. Furthermore, in the absence of sources, that is, $r = s = 0, \mathbf{f} = 0$, conservation of global phase and volumetric fluid content as well as energy dissipation holds.

The proof of this result will be considered in the next section. We note that the time-average strategy could also be applied to the whole system. The resulting scheme would preserve the energy-dissipation balance without numerical dissipation, cf. [36] where this strategy was applied to the Cahn-Hilliard equation.

Lemma 3.1. *The numerical discretization of the Cahn-Hilliard-Biot system as stated in Problem 1 can be realized as a decoupled scheme where the first step is linear, while the second step is, in general, nonlinear. The decoupled scheme reads as follows*:

Problem 2. Let $(\phi_h^n, \mathbf{u}_h^n, \theta_h^n) \in \mathcal{V}_h \times \mathcal{X}_h^d \times \mathcal{V}_h$ be given.

1. Find $(\mathbf{u}_h^{n+1}, \theta_h^{n+1}, p_h^{n+1}) \in \mathcal{X}_h^d \times \mathcal{V}_h \times \mathcal{V}_h$ such that

$$\begin{aligned}&\langle \mathbf{C}_v(\phi_h^n)\mathcal{E}(d_\tau^{n+1}\mathbf{u}_h), \mathcal{E}(\mathbf{v}_h)\rangle\\ &\quad + \langle \widetilde{W}_{\mathcal{E}(\mathbf{u})}(\phi_h^n, \mathcal{E}(\mathbf{u}_h^{n+1}), \theta_h^{n+1}), \mathcal{E}(\mathbf{v}_h)\rangle = \langle \mathbf{f}^{n+1}, \mathbf{v}\rangle\end{aligned} \tag{3.9}$$

$$\langle d_\tau^{n+1}\theta_h, \chi_h\rangle + \langle \kappa(\phi_h^n)\nabla p_h^{n+1}, \nabla\chi_h\rangle = \langle s(\phi_h^n, \mathcal{E}(\mathbf{u}_h^n), \theta_h^n), \chi_h\rangle \tag{3.10}$$

$$\langle p_h^{n+1}, q_h\rangle - \langle \widetilde{W}_\theta(\phi_h^n, \mathcal{E}(\mathbf{u}_h^{n+1}), \theta_h^{n+1}), q_h\rangle = 0 \tag{3.11}$$

holds for $(\mathbf{v}_h, \chi_h, q_h) \in \mathcal{X}_h^d \times \mathcal{V}_h \times \mathcal{V}_h$.

2. Find $(\phi_h^{n+1}, \mu_h^{n+1}) \in \mathcal{V}_h \times \mathcal{V}_h$ such that

$$\begin{aligned}&\langle d_\tau^{n+1}\phi_h, \psi_h\rangle + \langle m(\phi_h^n)\nabla\mu_h^{n+1}, \nabla\psi_h\rangle \\ &\quad = \langle r(\phi_h^n, \mathcal{E}(\mathbf{u}_h^{n+1}), \theta_h^{n+1}), \psi_h\rangle\end{aligned} \tag{3.12}$$

$$\begin{aligned}&\langle \mu_h^{n+1}, \xi_h\rangle - \gamma\langle\nabla\phi_h^{n+1}, \nabla\xi_h\rangle - \langle \Psi'(\phi_h^{n+1}, \phi_h^n), \xi_h\rangle \\ &- \langle \widetilde{W}_\phi^{av}(\phi_h, \mathcal{E}(\mathbf{u}_h^{n+1}), \theta_h^{n+1}), \xi_h\rangle = 0\end{aligned} \tag{3.13}$$

holds for $(\psi_h, \xi_h) \in \mathcal{V}_h \times \mathcal{V}_h$.

We note that the above scheme can be used similarly to approximate the Cahn-Hilliard-Larché system, that is, in the case $M \equiv 0$. Hence, we also provide a decoupling scheme for the Cahn-Hilliard-Larché system.

Proof. Careful inspection of Equations (3.1–3.5) reveal that the poro-elastic subsystem (3.3–3.5) does not depend on ϕ_h^{n+1} but only on ϕ_h^n. Hence, one can solve this subsystem and use the obtained solutions $\mathbf{u}_h^{n+1}$ and θ_h^{n+1} to solve the Cahn-Hilliard subsystem (3.1) and (3.2). Note that, due to the special structure of the energy, $\widetilde{W}_{\mathcal{E}(\mathbf{u})}(\phi_h^n, \mathcal{E}(\mathbf{u}_h^{n+1}), \theta_h^{n+1})$ and $\widetilde{W}_\theta(\phi_h^n, \mathcal{E}(\mathbf{u}_h^{n+1}), \theta_h^{n+1})$ are linear in $\mathcal{E}(\mathbf{u}_h^{n+1})$ and θ_h^{n+1}. □

We note that the discretization of the source terms r and s is chosen as above for specific reasons. First, the explicit choice in s leads to a linear discretization for the poro-elastic system. Second, the explicit evaluation of ϕ in r is chosen to prove the uniqueness of discrete solutions. Indeed, for an implicit evaluation the uniqueness proof does not work, and one has to resort to other approaches, as done in [37] for a Cahn-Hilliard equation that is coupled to a reaction-diffusion equation.

4 | Proof of Theorem 1

In this section, we prove Theorem 1 which states the existence of a solution to Problem 1 (and equivalently Problem 2 by Lemma 3.1), the conservation of phase and volumetric fluid content, the energy-dissipation balance, and the uniqueness of the solution for a CFL-type condition. We begin by proving the balance laws (3.6–3.8).

4.1 | Balance Laws

Regarding the balance of phase for ϕ_h, see (3.6), we insert the test function $\psi_h = 1$ in the equation that governs ϕ_h in the decoupled scheme; see (3.13). Thus, we obtain

$$\begin{aligned}\langle \phi_h, 1\rangle\big|_{t^n}^{t^{n+1}} &= \int_{I_n} \langle \partial_t\phi_h, 1\rangle = \int_{I_n} \langle d_\tau^{n+1}\phi_h, 1\rangle \\ &= -\int_{I_n} \big\langle m(\phi_h^n)\nabla\mu_h^{n+1}, \nabla 1\big\rangle + \int_{I_n} \big\langle r(\phi_h^n, \mathcal{E}(\mathbf{u}_h^{n+1}), \theta_h^{n+1}), 1\big\rangle \\ &= \tau\big\langle r(\phi_h^n, \mathcal{E}(\mathbf{u}_h^{n+1}), \theta_h^{n+1}), 1\big\rangle\end{aligned}$$

Summation over the relevant time steps yields the result (3.6). With the same computations using $\chi_h = 1$ in (3.10), we obtain the balance of volumetric fluid content (3.7), that is,

$$\langle \theta_h, 1\rangle\big|_{t^n}^{t^{n+1}} = \int_{I_n} \langle d_\tau^{n+1}\theta_h, 1\rangle = \tau\langle s(\phi_h^n, \mathcal{E}(\mathbf{u}_h^n), \theta_h^n), 1\rangle$$

Let us now prove the energy-dissipation balance as stated in (3.8). We have

$$\begin{aligned}\frac{1}{\tau}\mathcal{F}(\phi_h, \mathcal{E}(\mathbf{u}_h), \theta_h)\big|_{t^n}^{t^{n+1}} &= \gamma\langle\nabla\phi^{n+1}, d_\tau^{n+1}\nabla\phi_h\rangle + \langle \Psi'(\phi_h^{n+1}, \phi_h^n), d_\tau^{n+1}\phi_h\rangle \\ &\quad + \frac{1}{\tau}\langle \widetilde{W}(\phi_h^{n+1}, \mathcal{E}(\mathbf{u}_h^{n+1}), \theta_h^{n+1}) - \widetilde{W}(\phi_h^n, \mathcal{E}(\mathbf{u}_h^n), \theta_h^n), 1\rangle \\ &\quad + \frac{\tau\gamma}{2}\|\nabla d_\tau^{n+1}\phi_h\|_0^2 \\ &\quad + \frac{1}{\tau}\langle \Psi(\phi_h^{n+1}) - \Psi(\phi_h^n) - \Psi'(\phi_h^{n+1}, \phi_h^n)d^{n+1}\phi_h, 1\rangle \\ &= (a) + (b) + (c) + (d) + (e),\end{aligned}$$

where we introduced the short notation (a)–(e) for the five terms on the right-hand side. We consider each term and try to simplify them. We start with the third inner product called (c) by adding $\pm\langle \widetilde{W}(\phi_h^n, \mathcal{E}(\mathbf{u}_h^{n+1}), \theta_h^{n+1}), 1\rangle$, we find

$$\begin{aligned}(c) &= \frac{1}{\tau}\langle \widetilde{W}(\phi_h^{n+1}, \mathcal{E}(\mathbf{u}_h^{n+1}), \theta_h^{n+1}) - \widetilde{W}(\phi_h^n, \mathcal{E}(\mathbf{u}_h^{n+1}), \theta_h^{n+1}), 1\rangle \\ &\quad + \frac{1}{\tau}\langle \widetilde{W}(\phi_h^n, \mathcal{E}(\mathbf{u}_h^{n+1}), \theta_h^{n+1}) - \widetilde{W}(\phi_h^n, \mathcal{E}(\mathbf{u}_h^n), \theta_h^n), 1\rangle \\ &= \frac{1}{\tau}\int_{I_n} \partial_t\widetilde{W}(\phi_h, \mathcal{E}(\mathbf{u}_h^{n+1}), \theta_h^{n+1})\,\mathrm{d}s \\ &\quad + \frac{1}{\tau}\langle \widetilde{W}(\phi_h^n, \mathcal{E}(\mathbf{u}_h^{n+1}), \theta_h^{n+1}) - \widetilde{W}(\phi_h^n, \mathcal{E}(\mathbf{u}_h^n), \theta_h^n), 1\rangle\end{aligned}$$

Computing the time derivative and adding $\pm\langle \widetilde{W}_{\mathcal{E}(\mathbf{u})}(\phi_h^n, \mathcal{E}(\mathbf{u}_h^{n+1}), \theta_h^{n+1}), \mathcal{E}(d_\tau^{n+1}\mathbf{u}_h)\rangle$ and $\pm\langle \widetilde{W}_\theta(\phi_h^n, \mathcal{E}(\mathbf{u}_h^{n+1}), \theta_h^{n+1}), d_\tau^{n+1}\theta_h\rangle$ yields

$$\begin{aligned}(c) &= \frac{1}{\tau}\int_{I_n} \langle \widetilde{W}_\phi(\phi_h, \mathcal{E}(\mathbf{u}_h^{n+1}), \theta_h^{n+1}), \partial_t\phi_h\rangle\,\mathrm{d}s \\ &\quad + \langle \widetilde{W}_{\mathcal{E}(\mathbf{u})}(\phi_h^n, \mathcal{E}(\mathbf{u}_h^{n+1}), \theta_h^{n+1}), \mathcal{E}(d_\tau^{n+1}\mathbf{u}_h)\rangle \\ &\quad + \langle \widetilde{W}_\theta(\phi_h^n, \mathcal{E}(\mathbf{u}_h^{n+1}), \theta_h^{n+1}), d_\tau^{n+1}\theta_h\rangle \\ &\quad + \frac{1}{\tau}\langle \widetilde{W}(\phi_h^n, \mathcal{E}(\mathbf{u}_h^{n+1}), \theta_h^{n+1}) - \widetilde{W}(\phi_h^n, \mathcal{E}(\mathbf{u}_h^n), \theta_h^n) \\ &\quad - \widetilde{W}_{\mathcal{E}(\mathbf{u})}(\phi_h^n, \mathcal{E}(\mathbf{u}_h^{n+1}), \theta_h^{n+1})\mathcal{E}(d^{n+1}\mathbf{u}_h) \\ &\quad - \widetilde{W}_\theta(\phi_h^n, \mathcal{E}(\mathbf{u}_h^{n+1}), \theta_h^{n+1}), d^{n+1}\theta_h, 1\rangle \\ &= (i) + (ii) + (iii) + (iv)\end{aligned}$$

where we introduced the short notation (i)–(iv) for the terms on the right-hand side.

We note that since the time derivative is piecewise constant on I_n and coincides with the discrete time derivative $\partial_t\phi_h\big|_{I_n} = d_\tau^{n+1}\phi_h$, we can expand (i) as

$$\begin{aligned}(i) &= \left\langle \frac{1}{\tau}\int_{I_n} \widetilde{W}_\phi(\phi_h, \mathcal{E}(\mathbf{u}_h^{n+1}), \theta_h^{n+1})\quad \mathrm{d}s, d_\tau^{n+1}\phi_h\right\rangle \\ &= \langle \widetilde{W}_\phi^{av}(\phi_h, \mathcal{E}(\mathbf{u}_h^{n+1}), \theta_h^{n+1}), d_\tau^{n+1}\phi_h\rangle\end{aligned}$$

The addition of (a), (b), (i), (ii), (iii) yields

$$\begin{aligned}(A) = \gamma\langle\nabla\phi^{n+1}, d_\tau^{n+1}\nabla\phi_h\rangle + \langle\Psi'(\phi_h^{n+1}, \phi_h^n), d_\tau^{n+1}\phi_h\rangle \\ + \langle\widetilde{W}_\phi^{av}(\phi_h, \mathcal{E}(\mathbf{u}_h^{n+1}), \theta_h^{n+1}), d_\tau^{n+1}\phi_h\rangle \\ + \langle\widetilde{W}_{\mathcal{E}(\mathbf{u})}(\phi_h^n, \mathcal{E}(\mathbf{u}_h^{n+1}), \theta_h^{n+1}), \mathcal{E}(d_\tau^{n+1}\mathbf{u}_h)\rangle \\ + \langle\widetilde{W}_\theta(\phi_h^n, \mathcal{E}(\mathbf{u}_h^{n+1}), \theta_h^{n+1}), d_\tau^{n+1}\theta_h\rangle\end{aligned}$$

The addition of the remaining terms, that is, (d), (e) and (iv), yields

$$\begin{aligned}(B) = \frac{\tau\gamma}{2}\|\nabla d_\tau^{n+1}\phi_h\|_0^2 \\ + \frac{1}{\tau}\langle\Psi(\phi_h^{n+1}) - \Psi(\phi_h^n) - \Psi'(\phi_h^{n+1}, \phi_h^n)d^{n+1}\phi_h, 1\rangle \\ + \frac{1}{\tau}\langle\widetilde{W}(\phi_h^n, \mathcal{E}(\mathbf{u}_h^{n+1}), \theta_h^{n+1}) - \widetilde{W}(\phi_h^n, \mathcal{E}(\mathbf{u}_h^n), \theta_h^n) \\ - \widetilde{W}_{\mathcal{E}(\mathbf{u})}(\phi_h^n, \mathcal{E}(\mathbf{u}_h^{n+1}), \theta_h^{n+1})\mathcal{E}(d^{n+1}\mathbf{u}_h) \\ - \widetilde{W}_\theta(\phi_h^n, \mathcal{E}(\mathbf{u}_h^{n+1}), \theta_h^{n+1})d^{n+1}\theta_h, 1\rangle\end{aligned}$$

It remains to expand (A) and (B), and we will show that (A) gives rise to the dissipation and source rate, while (B) is the numerical dissipation, which is non-negative. We start with (A) and using as test functions $\xi_h = d_\tau^{n+1}\phi_h \in \mathcal{V}_h$ in (3.13) and $q_h = d_\tau^{n+1}\theta_h \in \mathcal{V}_h$ in (3.11) yields

$$\begin{aligned}(A) = \langle\mu_h^{n+1}, d_\tau^{n+1}\phi_h\rangle \\ + \langle\widetilde{W}_{\mathcal{E}(\mathbf{u})}(\phi_h^n, \mathcal{E}(\mathbf{u}_h^{n+1}), \theta_h^{n+1}), \mathcal{E}(d_\tau^{n+1}\mathbf{u}_h)\rangle + \langle p_h^{n+1}, d_\tau^{n+1}\theta_h\rangle\end{aligned}$$

Insertion of $\psi_h = \mu_h^{n+1} \in \mathcal{V}_h$ in (3.12), $\mathbf{v}_h = d_\tau^{n+1}\mathbf{u}_h \in \mathcal{X}_h^d$ in (3.9), and $\chi_h = p_h^{n+1} \in \mathcal{V}_h$ in (3.10) yields

$$\begin{aligned}= -\langle m(\phi_h)\nabla\mu_h^{n+1}, \nabla\mu_h^{n+1}\rangle - \langle\mathbf{C}(\phi_h^n)\mathcal{E}(d_\tau^{n+1}\mathbf{u}_h), \mathcal{E}(d_\tau^{n+1}\mathbf{u}_h)\rangle \\ - \langle\kappa(\phi_h^n)\nabla p_h^{n+1}, \nabla p_h^{n+1}\rangle \\ + \langle r^{n,n+1}, \mu_h^{n+1}\rangle + \langle\mathbf{f}, d_\tau^{n+1}\mathbf{u}_h\rangle + \langle s^n, p_h^{n+1}\rangle \\ = \mathcal{D}_{\phi_h^n}(\mu_h^{n+1}, d_\tau^{n+1}\mathbf{u}_h, p_h^{n+1}) + \int_{t^n}^{t^{n+1}} \mathcal{P}^*(\mu_h^{n+1}, d_\tau^{n+1}\mathbf{u}_h, p_h^{n+1}) \quad (4.1)\end{aligned}$$

where we defined the abbreviations $r^{n,n+1} := r(\phi_h^n, \mathcal{E}(\mathbf{u}_h^{n+1}), \theta_h^{n+1})$ and $s^n := s(\phi_h^n, \mathcal{E}(\mathbf{u}_h^n), \theta_h^n)$. Furthermore, we used the definitions of the dissipation and source rates as introduced in Lemma 2.1 and Theorem 1.

Hence, (A) corresponds to the usual variational structure of the problem and produces the dissipation and source rates. Next, we turn to (B) and by utilizing Taylor's expansion, we find

$$\begin{aligned}(B) = -\frac{\tau\gamma}{2}\|\nabla d_\tau^{n+1}\phi_h\|_0^2 - \frac{\tau}{2}\langle(\Psi''_{vex}(z_1) - \Psi''_{cav}(z_2))d_\tau^{n+1}\phi_h, d_\tau^{n+1}\phi_h\rangle \\ - \frac{\tau}{2}\langle\mathbf{H}_{\widetilde{W},\mathcal{E}(\mathbf{u}),\theta}(\phi_h^n, \mathbf{z}_3)(\mathcal{E}(d_\tau^{n+1}\mathbf{u}_h), d_\tau^{n+1}\theta_h)^\top \\ (\mathcal{E}(d_\tau^{n+1}\mathbf{u}_h), d_\tau^{n+1}\theta_h)^\top\rangle \quad (4.2)\end{aligned}$$

where z_1, z_2 are convex combinations of ϕ_h^n, ϕ_h^{n+1}, while $\mathbf{z}_3$ is a convex combination of $(\mathcal{E}(\mathbf{u}_h^{n+1}), \theta_h^{n+1})^\top$ and $(\mathcal{E}(\mathbf{u}_h^n), \theta_h^n)^\top$. Furthermore, $\mathbf{H}_{\widetilde{W},\mathcal{E}(\mathbf{u}),\theta}$ denotes the Hessian of $\widetilde{W}$ with respect to $\mathcal{E}(\mathbf{u})$ and θ. We recall that $\widetilde{W}$, cf. (2.4), is convex and thus yields $(B) \leq 0$. This finishes the energy-dissipation balance; see (3.8).

4.2 | A Priori Bounds

To prove the existence of a solution to Problem 1, we derive a priori bounds from the energy-dissipation balance.

Recalling the energy-dissipation balance (3.8) and using the assumptions (A3)–(A6) on the lower bounds of the system's functions, we find

$$\begin{aligned}\mathcal{F}(\phi_h^{n+1}, \mathcal{E}(\mathbf{u}_h^{n+1}), \theta_h^{n+1}) \\ + \tau\left(m_0\|\nabla\mu_h^{n+1}\|_0^2 + c\|\mathcal{E}(d_\tau^{n+1}\mathbf{u}_h)\|_0^2 + \kappa_0\|\nabla p_h^{n+1}\|_0^2\right) \\ \leq \mathcal{F}(\phi_h^n, \mathcal{E}(\mathbf{u}_h^n), \theta_h^n) \\ + \tau(\langle r^{n,n+1}, \mu_h^{n+1}\rangle + \langle\mathbf{f}^{n+1}, \mathcal{E}(d_\tau^{n+1}\mathbf{u}_h)\rangle + \langle s^n, p_h^{n+1}\rangle)\end{aligned}$$

Next, we estimate a lower bound for $\mathcal{F}(\phi_h^{n+1}, \mathcal{E}(\mathbf{u}_h^{n+1}), \theta_h^{n+1})$ and an upper bound for $\mathcal{F}(\phi_h^n, \mathbf{u}_h^n, \theta_h^n)$. First, using positivity of Ψ and the assumptions (A3) and (A6) we find

$$\begin{aligned}\mathcal{F}(\phi_h^{n+1}, \mathcal{E}(\mathbf{u}_h^{n+1}), \theta_h^{n+1}) \\ \geq \frac{\gamma}{2}\|\nabla\phi_h^{n+1}\|_0^2 + C_{\mathbf{u}}\|\mathbf{u}_h^{n+1}\|_1^2 - C(\|\phi_h^{n+1}\|_0^2 + 1) \\ + \frac{M_0}{2}\|\theta_h^{n+1} - \alpha(\phi_h^{n+1})\mathrm{div}(\mathbf{u}_h^{n+1})\|_0^2\end{aligned}$$

Following the computations in [2], we can estimate the right-hand side further to obtain

$$\begin{aligned}\mathcal{F}(\phi_h^{n+1}, \mathcal{E}(\mathbf{u}_h^{n+1}), \theta_h^{n+1}) \geq \frac{\gamma}{2}\|\nabla\phi_h^{n+1}\|_0^2 \\ + \left(C_{\mathbf{u}} - \frac{M_0}{2}\alpha_0^2\left(\frac{1}{\delta_\theta} - 1\right)\right)\|\mathbf{u}_h^{n+1}\|_1^2 - C(\|\phi_h^{n+1}\|_0^2 + 1) \\ + \frac{M_0}{2}(1 - \delta_\theta)\|\theta_h^{n+1} - \alpha(\phi_h^{n+1})\mathrm{div}(\mathbf{u}_h^{n+1})\|_0^2 \quad (4.3)\end{aligned}$$

Regarding the upper bound of $\mathcal{F}(\phi_h^n, \mathcal{E}(\mathbf{u}_h^n), \theta_h^n)$, we estimate using the assumptions (A3)–(A6)

$$\begin{aligned}\mathcal{F}(\phi_h^n, \mathcal{E}(\mathbf{u}_h^n), \theta_h^n) \leq \frac{\gamma}{2}\|\nabla\phi_h^n\|_0^2 + \|\Psi(\phi_h^n)\|_{0,1}^2 \\ + C\|\mathbf{u}_h^n\|_1^2 + C(\|\phi_h^n\|_0^2 + 1) + C\|\theta_h^n\|_0^2 \quad (4.4)\end{aligned}$$

Next, we insert $\psi_h = \beta\phi_h^{n+1}$ in (3.12), which gives

$$\begin{aligned}\frac{\beta}{2}\|\phi_h^{n+1}\|_0^2 + \frac{\beta}{2}\|d_\tau^{n+1}\phi_h\|_0^2 \\ \leq \frac{\beta}{2}\|\phi_h^n\|_0^2 + \tau m_0\|\nabla\mu_h^{n+1}\|_0\|\nabla\phi_h^{n+1}\|_0 + \tau\|r^{n,n+1}\|_0\|\phi_h^{n+1}\|_0 \quad (4.5)\end{aligned}$$

Combining the estimates (4.3–4.5) and choosing $\delta_\theta \leq 1 - \varepsilon$ and $\beta \geq 2C$, we find

$$\begin{aligned}C_a\left(\|\phi_h^{n+1}\|_1^2 + \|\mathbf{u}_h^{n+1}\|_1^2 + \|\theta_h^{n+1}\|_0^2\right) \\ + \tau\left(m_0\|\nabla\mu_h^{n+1}\|_0^2 + c_0\|d_\tau^{n+1}\mathbf{u}_h\|_1^2 + \kappa_0\|\nabla p_h^{n+1}\|_0^2\right) \\ \leq C_b\left(\|\phi_h^n\|_1^2 + \|\mathbf{u}_h^n\|_1^2 + \|\theta_h^n\|_0^2\right) \\ + \tau\left(\langle r^{n,n+1}, \mu_h^{n+1}\rangle + \langle\mathbf{f}^{n+1}, d_\tau^{n+1}\mathbf{u}_h\rangle + \langle s^n, p_h^{n+1}\rangle\right) \quad (4.6)\end{aligned}$$

It remains to treat the production terms and the external forces on the right-hand side of the inequality (4.6). First, we estimate the forces as follows:

$$\begin{aligned}\langle \mathbf{f}^{n+1}, d_\tau^{n+1}\mathbf{u}_h\rangle &\le \|\mathbf{f}^{n+1}\|_{-1}\|d_\tau^{n+1}\mathbf{u}_h\|_1 \\ &\le \frac{c_0}{2}\|d_\tau^{n+1}\mathbf{u}_h\|_1^2 + C\|\mathbf{f}^{n+1}\|_{-1}^2 \end{aligned} \tag{4.7}$$

$$\begin{aligned}\langle s^n, p_h^{n+1}\rangle &\le \|s^n\|_0\|p_h^{n+1}\|_0 \\ &\le C\|\theta_h^{n+1}\|_0^2 + C\|\mathbf{u}_h^{n+1}\|_1^2 + C\|s^n\|_0^2 \end{aligned} \tag{4.8}$$

Furthermore, the production term in the Cahn-Hilliard equation gives

$$\begin{aligned}\langle r^{n,n+1}, \mu_h^{n+1}\rangle &= \langle r^{n,n+1}, \mu_h^{n+1} - \langle \mu_h^{n+1}, 1\rangle\rangle + \langle r^{n,n+1}, \langle \mu_h^{n+1}, 1\rangle\rangle \\ &\le C(\delta)\|r^{n,n+1}\|_0^2 + \delta m_0\|\nabla\mu_h^{n+1}\|^2 + \delta\langle \mu_h^{n+1}, 1\rangle^2 \end{aligned} \tag{4.9}$$

Since we assumed that r is bounded, see (A7), it remains to estimate the squared mean value of μ_h^{n+1} in the last term of the inequality. This is done as follows using (A2):

$$\begin{aligned}\langle \mu_h^{n+1}, 1\rangle^2 &\le \|\Psi'_{vex}(\phi_h^{n+1})\|_{0,1}^2 + \|\Psi'_{cav}(\phi_h^n)\|_{0,1}^2 \\ &\quad + \|\widetilde{W}_\phi^{av}(\phi_h, \mathcal{E}(\mathbf{u}_h^{n+1}), \theta_h^{n+1})\|_{0,1}^2 \\ &\le C\left(\|\phi_h^{n+1}\|_1^2 + \|\phi_h^n\|_1^2\right) + C(\|\widetilde{W}_\phi(\phi_h^n, \mathcal{E}(\mathbf{u}_h^{n+1}), \theta_h^{n+1})\|_{0,1}^2 \\ &\quad + \|\widetilde{W}_\phi(\phi_h^{n+1}, \mathcal{E}(\mathbf{u}_h^{n+1}), \theta_h^{n+1})\|_{0,1}^2) \end{aligned}$$

Next, we estimate the two norms on the right-hand side that involve the derivative of the functional $\widetilde{W}$ with respect to ϕ. Using its structure, see (2.4), we find for $\phi_h^* \in \{\phi_h^{n+1}, \phi_h^n\}$ that

$$\begin{aligned}&\|\widetilde{W}_\phi(\phi_h^*, \mathcal{E}(\mathbf{u}_h^{n+1}), \theta_h^{n+1})\|_{0,1}^2 \\ &\quad \le \|\mathcal{E}(\mathbf{u}_h^{n+1}) - \mathcal{T}(\phi_h^*)\|_0^2 + \|\mathcal{T}'(\phi_h^*)\|_0^2 + C\|\theta_h^{n+1}\|_0^2 + \|\mathbf{u}_h^{n+1}\|_1^2 \\ &\quad \le C\|\mathcal{E}(\mathbf{u}_h^{n+1})\|_0^2 + C\|\phi_h^*\|_0^2 + C\|\theta_h^{n+1}\|_0^2 + \|\mathbf{u}_h^{n+1}\|_1^2 \end{aligned} \tag{4.10}$$

Combining all estimates, i.e. (4.7–4.10) and inserting them back into (4.6), we find that

$$\begin{aligned}&(C_a - C\tau)\left(\|\phi_h^{n+1}\|_1^2 + \|\mathbf{u}_h^{n+1}\|_1^2 + \|\theta_h^{n+1}\|_0^2\right) \\ &\quad + \tau\left(m_0\|\nabla\mu_h^{n+1}\|_0^2 + c_0\|d_\tau^{n+1}\mathbf{u}_h\|_1^2 + \kappa_0\|\nabla p_h^{n+1}\|_0^2\right) \\ &\le (C_b + C\tau)\left(\|\phi_h^n\|_1^2 + \|\mathbf{u}_h^n\|_1^2 + \|\theta_h^n\|_0^2\right) \\ &\quad + C\tau\left(\|r^{n,n+1}\|_0^2 + \|s^n\|_0^2 + \|\mathbf{f}^{n+1}\|_{-1}^2\right) \end{aligned}$$

At this point, we choose the step size $\tau \le \frac{C_a}{2C}$, so that we can write the above problem as

$$y^{n+1} + \tau D^{n+1} \le Cy^n + \tau g^n$$

where we have defined

$$\begin{aligned} y^k &:= \|\phi_h^k\|_1^2 + \|\mathbf{u}_h^k\|_1^2 + \|\theta_h^k\|_0^2 \\ D^{n+1} &:= m_0\|\nabla\mu_h^{n+1}\|_0^2 + c_0\|d_\tau^{n+1}\mathbf{u}_h\|_1^2 + \kappa_0\|\nabla p_h^{n+1}\|_0^2, \\ g^n &:= C\left(\|r^{n,n+1}\|_0^2 + \|s^n\|_0^2 + \|\mathbf{f}^{n+1}\|_{-1}^2\right) \end{aligned}$$

We sum over the first n time-steps and apply an immediate consequence of the discrete Gronwall lemma, see [38, Lemma 2.2], which yields

$$\begin{aligned}&\frac{C_a}{2}\left(\|\phi_h^{n+1}\|_1^2 + \|\mathbf{u}_h^{n+1}\|_1^2 + \|\theta_h^{n+1}\|_0^2\right) \\ &\quad + \sum_{k=0}^{n-1}\tau\left(m_0\|\nabla\mu_h^{k+1}\|_0^2 + c_0\|d_\tau^{k+1}\mathbf{u}_h\|_1^2 + \kappa_0\|\nabla p_h^{k+1}\|_0^2\right) \\ &\le C^*(\|\phi_h^0\|_1^2 + \|\mathbf{u}_h^0\|_1^2 + \|\theta_h^0\|_0^2) \\ &\quad + \sum_{k=0}^{n-1}\tau C(\|r^{k,k+1}\|_0^2 + \|s^k\|_0^2 + \|\mathbf{f}^{k+1}\|_{-1}^2) \end{aligned} \tag{4.11}$$

Due to assumption (A7), the terms involving r, s, and $\mathbf{f}$ are uniformly bounded in the respective norms. Thus, we obtain the desired a priori bound.

4.3 | Existence

We consider the n-th time step and assume that $\phi_h^{n-1}, \mathbf{u}_h^{n-1}$ and θ_h^{n-1} are already known. After choosing a basis for $\mathcal{V}_h \times \mathcal{V}_h \times \mathcal{X}_h^d \times \mathcal{V}_h \times \mathcal{V}_h$, we rewrite the variational system (3.1–3.5) as a nonlinear system in the form of

$$J(x) = 0 \text{ in } \mathbb{R}^Z$$

with $Z = \dim(\mathcal{V}_h)^4 \times \dim(\mathcal{X}_h)^d$. In fact, writing $\langle J(x), x\rangle$ is equivalent to testing the corresponding variational identities with

$$x = (\mu_h^{n+1} + \beta\phi_h^{n+1}, d_\tau^{n+1}\phi_h, d_\tau^{n+1}\mathbf{u}_h, p_h^{n+1}, d_\tau^{n+1}\theta_h)$$

As a consequence of the latter, we thus obtain

$$\langle J(x), x\rangle \ge y^{n+1} - Cy^n + \tau D^{n+1} - \tau C$$

Using the same arguments as we have used to derive the a priori bound (4.11), we directly obtain

$$\langle J(x), x\rangle \to \infty \text{ for } |x| \to \infty$$

Thus, the existence of a solution follows from a corollary to Brouwer's fixed-point theorem; see [39, Proposition 2.8].

4.4 | Uniqueness

We consider one time step and recall Lemma 3.1, that is, the scheme can be formulated as a splitting scheme. For the sake of presentation, we will neglect the space discretization index h in the remaining part of the proof.

Since we already know that solutions exist see Section 4.3, the poro-elastic subsystem has a unique solution as it is linear. Hence, the triple $(\mathbf{u}^{n+1}, \theta^{n+1}, p^{n+1})$ is uniquely determined for a given triple $(\phi^n, \mathbf{u}^n, \theta^n)$. Regarding the Cahn-Hilliard subsystem, we assume that two different solutions $(\phi_1^{n+1}, \mu_1^{n+1})$ and $(\phi_2^{n+1}, \mu_2^{n+1})$ exist. We denote their differences by ϕ^{n+1} and μ^{n+1}. Taking the

difference in the variational forms yields the following discrete formulations:

$$\langle \phi^{n+1}, \psi \rangle + \tau \langle m(\phi_1^n) \nabla \mu^{n+1}, \nabla \psi \rangle = 0 \tag{4.12}$$

$$\begin{aligned} &\langle \mu^{n+1}, \xi \rangle - \gamma \langle \nabla \phi^{n+1}, \nabla \xi \rangle - \langle \Psi''_{vex}(\zeta) \phi^{n+1}, \xi \rangle \\ &\quad - \langle \widetilde{W}^{av}_{\phi\phi}(\zeta, \mathcal{E}(\mathbf{u}^{n+1}), \theta^{n+1}) \phi^{n+1}, \xi \rangle = 0 \end{aligned} \tag{4.13}$$

which holds for all $(\psi, \xi) \in \mathcal{V}_h \times \mathcal{V}_h$. Above, $\widetilde{W}^{av}_{\phi\phi}$ is defined as the difference of $\widetilde{W}^{av}_{\phi}$ evaluated at the two solution sets. In addition, we note that ζ is a convex combination of ϕ_1^{n+1} and ϕ_2^{n+1}.

In the following, we introduce the discrete inverse Laplacian with a mobility function in the spirit of [40]. We define the mean free space $\mathcal{G} := \{v \in (H^1(\Omega))' : \langle v, 1 \rangle = 0\}$ and the weighted inverse Laplacian $\Delta^{-1}_{h,m} : \mathcal{G} \to \mathcal{V}_h$, which is given by

$$\langle m(\phi_1^n) \nabla(-\Delta^{-1}_{h,m} v), \nabla w \rangle = \langle v, w \rangle$$

This operator defines a discrete $H^{-1}(\Omega)$-norm via

$$\|v\|^2_{-1,m} := \langle \nabla \Delta^{-1}_{h,m} v, \nabla \Delta^{-1}_{h} v \rangle = \langle m(\phi_1^n) \nabla(-\Delta^{-1}_{h,m} v), \nabla(-\Delta^{-1}_{h,m} v) \rangle$$

and an associated interpolation inequality is given by

$$\begin{aligned} \|v\|_0^2 = \langle v, v \rangle &= \langle m(\phi_1^n) \nabla(-\Delta^{-1}_{h,m} v), \nabla v \rangle \\ &\leq \| \sqrt{m(\phi_1^n)} \|_{0,\infty} \|v\|_{-1,h,m} \|\nabla v\|_0 \end{aligned}$$

Although ϕ_1^{n+1} and ϕ_2^{n+1} are not mean free, the difference ϕ^{n+1} is mean free by construction; see (4.12) with $\psi = 1$. Hence, we are allowed to apply the weighted inverse Laplacian on ϕ^{n+1}. Using $\psi = -\Delta^{-1}_{h,m} \phi^{n+1} \in \mathcal{V}_h$ and $\xi = \phi^{n+1} \in \mathcal{V}_h$ as test functions in (4.12) and (4.13), respectively, which yields

$$\begin{aligned} &\|\phi^{n+1}\|^2_{-1,m} + \tau \big(\|\nabla \phi^{n+1}\|_0^2 + \langle \Psi''_{vex}(\zeta) \phi^{n+1}, \phi^{n+1} \rangle \big) \\ &\quad = -\tau \langle \widetilde{W}^{av}_{\phi\phi}(\zeta, \mathcal{E}(\mathbf{u}^{n+1}), \theta^{n+1}) \phi^{n+1}, \phi^{n+1} \rangle \end{aligned} \tag{4.14}$$

It remains to estimate the right-hand side in a suitable manner. First, we observe that we can split $\widetilde{W}^{av}_{\phi\phi}$ on the right-hand side into two terms using the convex nature of ζ as follows:

$$\begin{aligned} &\left| \widetilde{W}^{av}_{\phi\phi}(\zeta, \mathcal{E}(\mathbf{u}^{n+1}), \theta^{n+1}) \right| \\ &\quad \leq C \left| \widetilde{W}_{\phi\phi}(\zeta^{n+1}, \mathcal{E}(\mathbf{u}^{n+1}), \theta^{n+1}) \right| + C \left| \widetilde{W}_{\phi\phi}(\zeta^{n}, \mathcal{E}(\mathbf{u}^{n+1}), \theta^{n+1}) \right| \\ &\quad =: (i) + (ii) \end{aligned}$$

Before proceeding with the estimates of the second term (ii) on the right-hand side of the above inequality, we note that we have assumed in Theorem 1 that $\mathcal{T}_h$ is quasi-uniform, that is, we can further resort to inverse inequalities, see [41, Theorem 4.5.11], of the following form

$$\|v_h\|_{H^1} \leq c_{\text{inv}} h^{-1} \|v_h\|_{L^2} \tag{4.15}$$

$$\|v_h\|_{L^p} \leq c_{\text{inv}} h^{d/p - d/q} \|v_h\|_{L^q} \tag{4.16}$$

which hold for all discrete functions $v_h \in \mathcal{V}_h$ and all $1 \leq q \leq p \leq \infty$. We note that the same estimates hold as well for functions in $\mathcal{X}_h$ and hence in $\mathcal{X}_h^d$.

With the above preparations, we estimate using assumption A3–A6

$$\begin{aligned} (i) &\leq \tau \langle |\widetilde{W}_{\phi\phi}|, (\phi^{n+1})^2 \rangle \\ &\leq \tau C \langle |\mathcal{E}(\mathbf{u}^{n+1})|^2 + |\zeta^{n+1}|^2 + |\theta^{n+1}|^2 + 1, (\phi^{n+1})^2 \rangle \\ &\leq \tau C (\|\mathbf{u}^{n+1}\|^2_{1,\infty} + \|\phi^{n+1}\|^2_{0,\infty} + \|\theta^{n+1}\|^2_{0,\infty}) \|\phi^{n+1}\|_0^2 \\ &\leq \tau C (\|\mathbf{u}^{n+1}\|^4_{1,\infty} + \|\phi^{n+1}\|^4_{0,\infty} + \|\theta^{n+1}\|^4_{0,\infty}) \|\phi^{n+1}\|^2_{-1,m} \\ &\quad + \frac{\gamma \tau}{4} \|\nabla \phi^{n+1}\|_0^2 \\ &\leq \tau h^{-2d} C (\|\mathbf{u}^{n+1}\|_1^4 + \|\phi^{n+1}\|_0^4 + \|\theta^{n+1}\|_0^4) \|\phi^{n+1}\|^2_{-1,m} \\ &\quad + \frac{\gamma \tau}{4} \|\nabla \phi^{n+1}\|_0^2 \\ &\leq \tau h^{-2d} C_1 \|\phi^{n+1}\|^2_{-1,m} + \frac{\gamma \tau}{4} \|\phi^{n+1}\|_0^2 \end{aligned}$$

where we used the inverse inequality (4.15) and the a priori estimate (4.11) in the last step to bound the term

$$\|\mathbf{u}^{n+1}\|_1^4 + \|\phi^{n+1}\|_0^4 + \|\theta^{n+1}\|_0^4$$

uniformly in h and τ. Using the assumed CFL-like condition $\tau \leq \frac{h^{2d}}{2C_1}$, we find that

$$(i) \leq \frac{1}{2} \|\phi^{n+1}\|^2_{-1,m} + \tau \frac{\gamma}{2} \|\phi^{n+1}\|_0^2$$

The term (ii) can be estimated in the same manner. Finally, inserting this estimate back into the inequality (4.14), we obtain

$$\frac{1}{2} \|\phi^{n+1}\|^2_{-1,m} + \tau \left(\frac{\gamma}{2} \|\nabla \phi^{n+1}\|_0^2 + \langle \Psi''_{vex}(\zeta) \phi^{n+1}, \phi^{n+1} \rangle \right) \leq 0$$

Hence, it holds $\phi^{n+1} = 0$ everywhere. It is straightforward to see that this also implies $\mu^{n+1} = 0$ everywhere, which yields a contradiction and implies the uniqueness result, as stated in Theorem 1. This finishes the proof.

5 | Numerical Illustrations

In this section, we illustrate the behavior of the scheme, see Problem 2, by numerical experiments similar to those shown in [1, 12]. First, we consider a convergence test showing the first-order convergence in space. Afterwards, we compare the Cahn-Hilliard-Biot model to the established Cahn-Hilliard-Larché equations when considering typical examples in tumor growth models; see [9]. The scheme is implemented in the high-performance multiphysics finite element software NGSolve [42].

The nonlinear system is treated with a Newton method with tolerance 10^{-10}. We note that it is generally not possible to compute the time averages exactly. Hence, we employ a sufficiently high quadrature rule, that is,

$$g^{av}(\rho) := \frac{1}{\tau} \int_{t^n}^{t^{n+1}} g(\rho(s)) \, \mathrm{d}s \approx \frac{1}{\tau} \sum_{i=1}^{M} \omega_i g(\rho(t_i))$$

We point out that piecewise linear functions can be parameterized via the new and old time steps as ϕ_h is piecewise linear in time. In the case where g is a polynomial in ϕ_h, these can be done exactly, which is the case here. As already assumed in (A2) for the analysis, we use the convex-concave splitting of the nonlinear potential $\Psi = \Psi_{\text{cav}} + \Psi_{\text{vex}}$ into its expansive Ψ_{cav} and contractive part Ψ_{vex}, see the initial work [43] where this splitting was used to prove the unconditional gradient stability of the Cahn-Hilliard equation. In the case of $\Psi(\phi) = \frac{1}{4}(1-\phi^2)^2$, we set $\Psi'_{\text{vex}}(\phi) = \phi^3$ and $\Psi'_{\text{cav}}(\phi) = \phi$. We treat the expansive part explicitly and the contractive part implicitly.

The material parameters can be found in Table 1. We note that the tensors are written in Voigt notation in two spatial dimensions. The parameter set is taken from [1]. Further, the permeability κ, compressibility M, Biot-Willis coefficient α, elasticity tensor $\mathbb{C}$, and consolidation tensor $\mathbb{C}_\nu$ depend on the phase field through the interpolation function π as follows:

$$\begin{aligned}
\kappa(\phi) &= \kappa_{-1} + \pi(\phi)(\kappa_1 - \kappa_{-1}) \\
M(\phi) &= M_{-1} + \pi(\phi)(M_1 - M_{-1}) \\
\alpha(\phi) &= \alpha_{-1} + \pi(\phi)(\alpha_1 - \alpha_{-1}) \\
\mathbb{C}(\phi) &= \mathbb{C}_{-1} + \pi(\phi)(\mathbb{C}_1 - \mathbb{C}_{-1}) \\
\mathbb{C}_\nu(\phi) &= \mathbb{C}_{\nu,-1} + \pi(\phi)(\mathbb{C}_{\nu,1} - \mathbb{C}_{\nu,-1})
\end{aligned}$$

Specifically, we choose the interpolation function

$$\pi(\phi) = \begin{cases} 0, & \phi < -1 \\ \frac{1}{4}(2 + 3\phi - \phi^3), & \phi \in [-1, 1] \\ 1, & \phi > 1 \end{cases}$$

TABLE 1 | Table of simulation parameters.

Symbol	Value	Symbol	Value
m	1	α_{-1}, α_1	1, 0.5
γ	10^{-4}	κ_{-1}, κ_1	1, 0.1
ξ	0.3	M_{-1}, M_1	1, 0.1
$\mathbf{C}_{-1}$	$\begin{pmatrix} 4 & 2 & 0 \\ 2 & 4 & 0 \\ 0 & 0 & 8 \end{pmatrix}$	$\mathbf{C}_1$	$\begin{pmatrix} 1 & 0.5 & 0 \\ 0.5 & 1 & 0 \\ 0 & 0 & 2 \end{pmatrix}$
$\mathbf{C}_{\nu,-1}$	$\begin{pmatrix} 1 & 0.5 & 0 \\ 0.5 & 1 & 0 \\ 0 & 0 & 2 \end{pmatrix}$	$\mathbf{C}_{\nu,1}$	$\begin{pmatrix} 1 & 0.5 & 0 \\ 0.5 & 1 & 0 \\ 0 & 0 & 2 \end{pmatrix}$

as originally chosen in [30] for the simulation of the Cahn-Hilliard-Larché equation. In addition, we choose the eigenstrain as $\mathcal{T}(\phi) = \zeta\phi\mathbf{I}$ with ζ given in Table 1.

5.1 | Convergence Test

We consider the error in space at the final time $T = 0.01$ with a respective time-step size of $\tau = 10^{-5}$ by comparing the numerical solutions $(\phi_h, \mu_h, \mathbf{u}_h, \theta_h, p_h)$ with those computed on uniformly refined grids, $(\phi_{h/2}, \mu_{h/2}, \mathbf{u}_{h/2}, \theta_{h/2}, p_{h/2})$ as no analytical solution to the Cahn-Hilliard-Biot system is available. The error quantities for the fully discrete scheme are defined by

$$\begin{aligned}
e_h = \|\phi_h - \phi_{h/2}\|^2_{H^1} + \|\mathcal{E}(\mathbf{u}_h) - \mathcal{E}(\mathbf{u}_{h/2})\|^2_{L^2} + \|\theta_h - \theta_{h/2}\|^2_{L^2} \\
+ \|\mu_h - \mu_{h/2}\|^2_{H^1} + \|p_h - p_{h/2}\|^2_{H^1}
\end{aligned}$$

as well as the separated errors $e^\phi_h, e^\mu_h, e^{\mathbf{u}}_h$ and e^p_h, which denote the related single quantities from the second error norm, e.g., $e^\phi_h = \|\phi_h - \phi_{h/2}\|^2_{H^1}$.

Experiment 1. We assume a smooth set of initial data given by

$$\phi_0 = -0.1 + 0.01\sin(2\pi x)\sin(2\pi y), \quad \mathbf{u}_0 = \mathbf{0}, \quad \theta_0 = 0,$$

and the source function $r = s = 0, \mathbf{f} = \mathbf{0}$.

For the spatial step sizes $h_k = 2^{-k}$ with $k \in \{2, \dots, 6\}$ of the domain $\Omega = (0,1)^2$ we obtain the error rates as illustrated in Table 2. We observe second-order convergence in the squared norms, which implies the expected first-order convergence in space.

5.2 | Validation Experiments

Experiment 2. We consider an initial condition with three bubbles of phase $\phi = 1$ while the rest of the domain $\Omega = (0,1)^2$ is given by $\phi = -1$ together with zero initial displacement and zero volumetric fluid content. Thus, we assume

$$\begin{aligned}
\phi_0 &= 2 - \tanh\left(\frac{\mathcal{B}(0.3, 0.3, 0.15)}{0.005}\right) - \tanh\left(\frac{\mathcal{B}(0.3, 0.7, 0.15)}{0.005}\right) \\
&\quad - \tanh\left(\frac{\mathcal{B}(0.7, 0.3, 0.15)}{0.005}\right), \\
\mathbf{u}_0 &= \mathbf{0}, \qquad \theta_0 = 0, \qquad \mathcal{B}(x_0, y_0, r) := (x - x_0)^2 + (y - y_0)^2 - r^2
\end{aligned}$$

with the source functions $r = s = 0, \mathbf{f} = \mathbf{0}$.

TABLE 2 | Errors and experimental orders of convergence (eoc).

k	e_h	eoc	e^ϕ_h	eoc	e^μ_h	eoc	$e^{\mathbf{u}}_h$	eoc	e^p_h	eoc
2	$1.23 \cdot 10^{-3}$	—	$1.20 \cdot 10^{-3}$	—	3.72×10^{-5}	—	6.80×10^{-8}	—	1.01×10^{-6}	—
3	6.27×10^{-4}	0.98	6.02×10^{-4}	0.99	2.19×10^{-5}	0.77	3.05×10^{-8}	1.16	5.23×10^{-7}	0.95
4	2.67×10^{-4}	1.23	2.57×10^{-4}	1.23	7.13×10^{-6}	1.62	7.86×10^{-9}	1.96	1.50×10^{-7}	1.80
5	6.64×10^{-5}	2.00	6.36×10^{-5}	2.02	1.79×10^{-6}	1.99	2.01×10^{-9}	1.97	3.75×10^{-8}	2.00
6	1.60×10^{-5}	2.05	1.51×10^{-5}	2.07	4.39×10^{-7}	2.03	5.07×10^{-10}	1.99	9.26×10^{-9}	2.02

We depict the result in Figure 1. One can clearly see that after a short time period at $t \approx 0.02$, the three bubbles merge and begin to agglomerate. This agglomeration process contrasts with the usual Cahn-Hilliard dynamics subjected to elastic contribution and results in the L shape, which expands over time, that is, at $t \approx 0.06$ and finally at $t \approx 2$. Note that this specific L shape is due to the special choice of the eigenstrain $\mathcal{T} = \zeta\phi\mathbf{I}$, which implies that the stress-free state is located at $\phi = 0$, that is, at the interface. Hence, the system tries to expose as much interface as possible given the contrary Cahn-Hilliard dynamics. The evolution of the energy as well as the conservation errors are depicted in Figure 2. Since r, f, s are zero, we expect and indeed observe energy dissipation, global phase, and volumetric fluid content conservation.

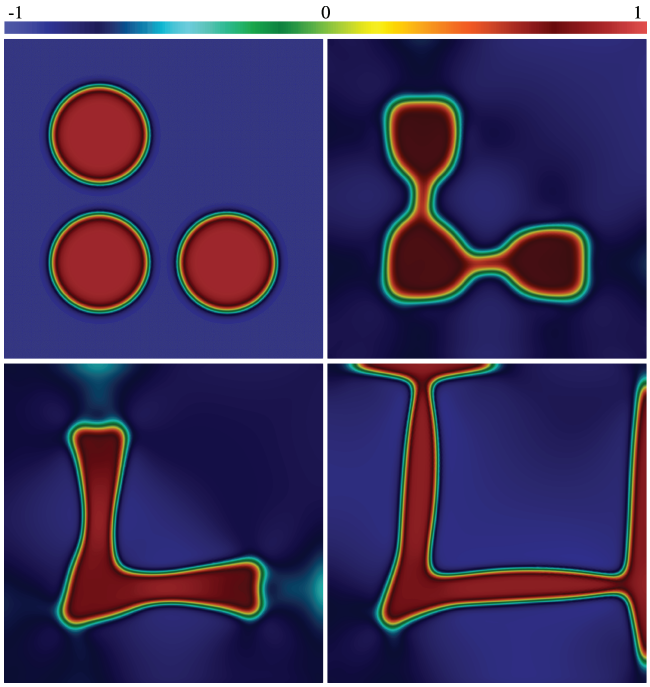

FIGURE 1 | Experiment 2: Snapshots of the phase field ϕ at the times $t \in \{0, 0.02, 0.06, 2\}$ with mesh size $h_{\max} \approx 10^{-2}$ and time-step $\tau = 10^{-3}$ (from top left to bottom right).

The next experiment is related to tumor growth. In this case, we compare the Cahn-Hilliard-Biot system (CHB) with the Cahn-Hilliard-Larché system (CHL), which is achieved by assuming compressibility $M = 0$. We recall that ϕ describes the difference in volume fractions, that is, $\{\phi = 1\}$ represents unmixed tumor tissue, while $\{\phi = -1\}$ represents surrounding healthy tissue.

Experiment 3. We consider a single bubble (here the tumor) parametrized by

$$\phi_0 = -\tanh\left(\frac{\mathcal{B}(0.5, 0.5, 0.15)}{0.005}\right), \qquad \mathbf{u}_0 = \mathbf{0}, \qquad \theta_0 = 0$$

Furthermore, we choose the logistic growth function $r(\phi) = \frac{5}{2}(1 - \phi^2)$, $s = \mathbf{f} = 0$ and mobility $m(\phi) = 10^{-14} + \frac{1}{16}(\phi^2 - 1)^2$. Additionally, the following parameters are changed in comparison to Table 1

$$\mathbb{C}_v = 0, \quad \mathcal{T}(\phi) = \frac{1}{2}\zeta(\phi + 1)\mathbf{I}, \quad \mathbf{C}_{-1} = \begin{pmatrix} 6 & 4 & 0 \\ 4 & 6 & 0 \\ 0 & 0 & 1 \end{pmatrix}$$

$$\mathbf{C}_1 = \begin{pmatrix} 1.55 & 0.38 & 0 \\ 0.38 & 1.55 & 0 \\ 0 & 0 & 0.58 \end{pmatrix}$$

Snapshots of these experiments are given in Figures 3–5. In Figure 3 we show the evolution of the CHB system, which appears to be very similar to the evolution of the CHL system in Figure 4. To highlight the difference, we also compute the difference between both solutions, that is, $|\phi_{\text{CHB}} - \phi_{\text{CHL}}|$ and plot it in Figure 5. From this, we see that both models agree very well apart from the interface, while on the interface we observe errors up to the order 10^{-3}. Since both systems start from the same data and the elastic/poro-elastic system is initialized with zero and $s = 0$, this suggests that the CHB system exhibits a distinct feature at the

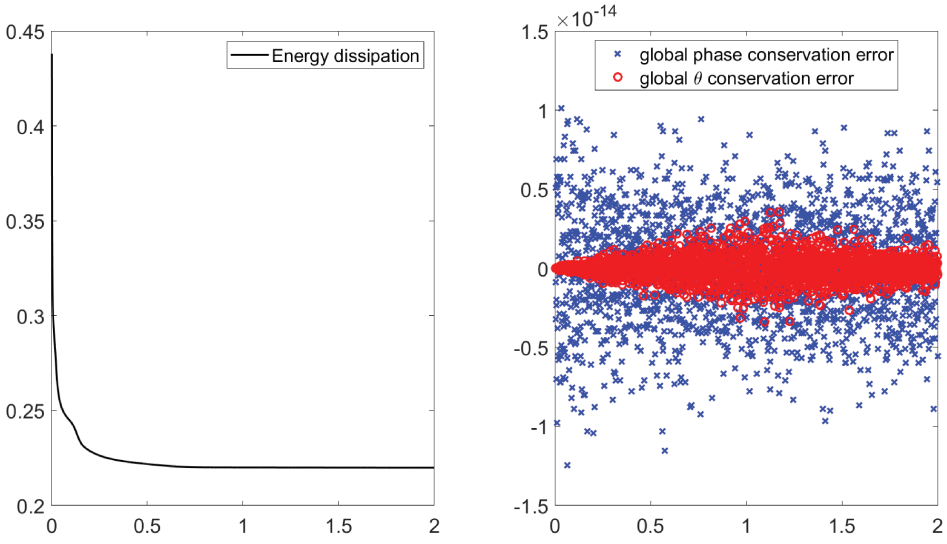

FIGURE 2 | Experiment 2: Temporal evolution of the energy (left) and the conservation errors (right).

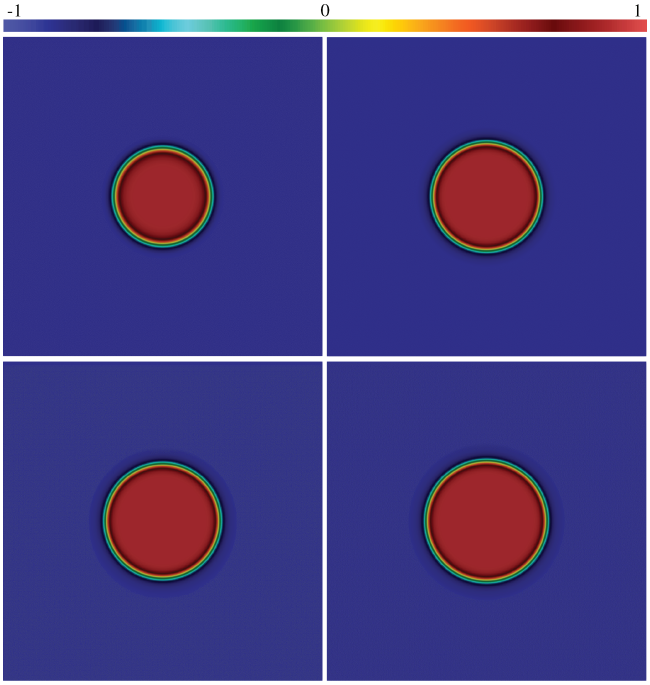

FIGURE 3 | Experiment 3 for the CHB system: Snapshots of the phase field ϕ at the times $t \in \{0, 0.5, 0.75, 1\}$ with mesh size $h_{\max} \approx 10^{-2}$ and time-step $\tau = 10^{-3}$ (from top left to bottom right).

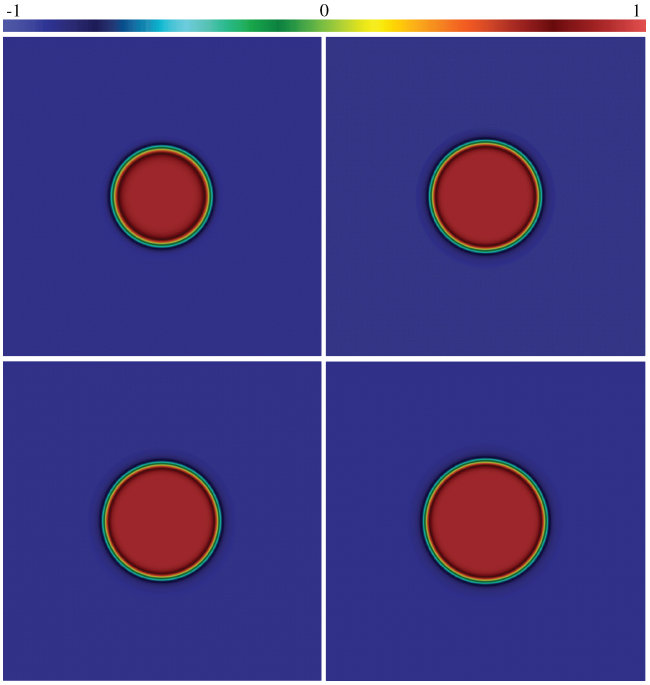

FIGURE 4 | Experiment 3 for the CHL system: Snapshots of the phase field ϕ at times $t \in \{0, 0.5, 0.75, 1\}$ with mesh size $h_{\max} \approx 10^{-2}$ and time-step $\tau = 10^{-3}$ (from top left to bottom right).

interface. This new interface behavior warrants further detailed investigation. The evolution of the energy as well as the conservation error are depicted in Figure 6. In this case we have only conservation of volumetric fluid content; energy as well as global phase is increasing.

The final example combines both experiments; that is, we consider tumor growth using three initial tumors in three space dimensions by choosing the domain $\Omega = (0, 1)^3$.

Experiment 4. We consider the following set of initial data:

$$\begin{aligned}\phi_0 &= 2 - \tanh\left(\frac{\mathcal{B}(0.3, 0.3, 0.3, 0.15)}{0.01}\right) \\ &\quad - \tanh\left(\frac{\mathcal{B}(0.3, 0.7, 0.3, 0.15)}{0.01}\right) \\ &\quad - \tanh\left(\frac{\mathcal{B}(0.7, 0.3, 0.3, 0.15)}{0.01}\right), \quad \mathbf{u}_0 = \mathbf{0}, \quad \theta_0 = 0 \\ \mathcal{B}(x_0, y_0, z_0, r) &:= (x - x_0)^2 + (y - y_0)^2 + (z - z_0)^2 - r^2.\end{aligned}$$

Furthermore, we choose $r(\phi) = \frac{5}{2}(1 - \phi^2)$, $s = \mathbf{f} = 0$ and $m(\phi) = 10^{-14} + \frac{1}{16}(\phi^2 - 1)^2$. Additionally, the following parameters are changed in comparison to Table 1

$$\mathbf{C}_{-1} = \begin{pmatrix} 6 & 4 & 0 \\ 4 & 6 & 0 \\ 0 & 0 & 1 \end{pmatrix}, \quad \mathbf{C}_1 = \begin{pmatrix} 1.55 & 0.38 & 0 \\ 0.38 & 1.55 & 0 \\ 0 & 0 & 0.58 \end{pmatrix}$$

$$\mathbb{C}_\nu = 10^{-2}\mathbf{C}_1, \quad \mathcal{T} = \frac{1}{2}\zeta(\phi + 1)\mathbf{I}$$

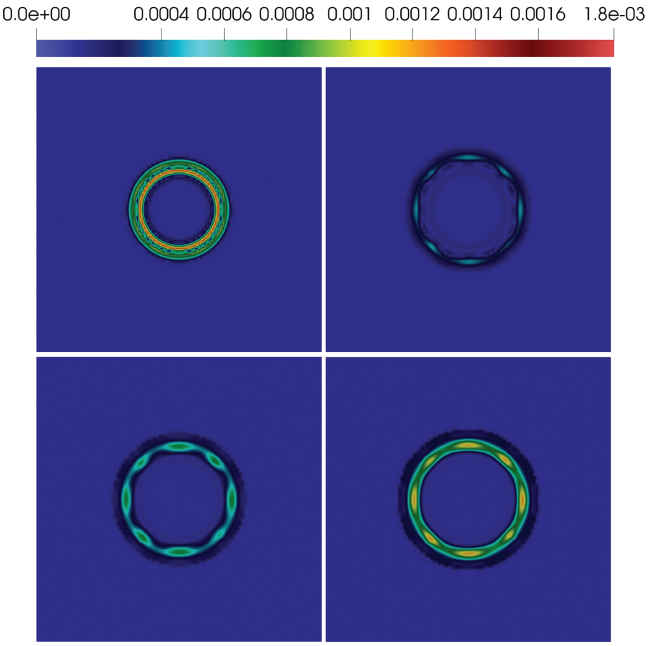

FIGURE 5 | Experiment 3: Difference between the phase-fields of the CHB and CHL solutions in the times $t \in \{0.01, 0.5, 0.75, 1\}$ (from top left to bottom right).

The simulation results are shown in Figure 7. The three initial bubbles start to grow over time and start to connect around $t \approx 0.8$. Afterwards, the agglomeration process starts, which can be seen at $t \approx 1$. Note that, as discussed in Experiment 2, due to the different choice of the eigenstrain $\mathcal{T}$, we do not observe the L shape in this simulation. Instead, the tumor keeps its circular

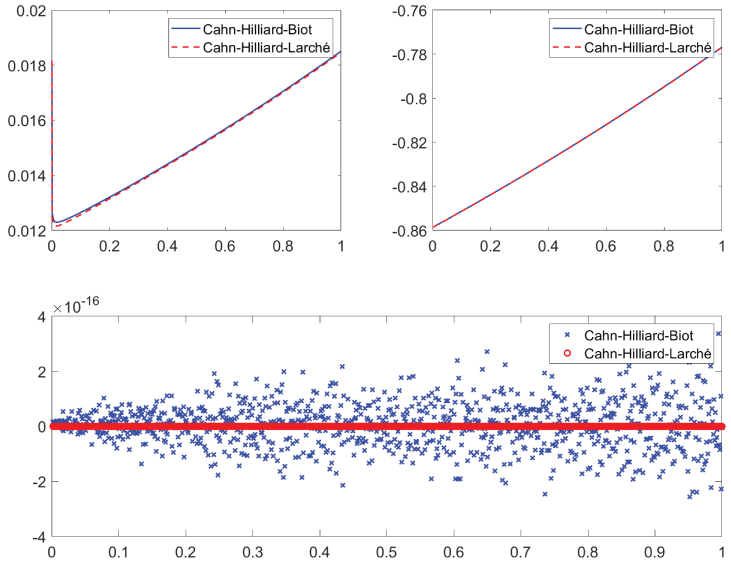

FIGURE 6 | Experiment 3: Temporal evolution of the energy (upper left) and global phase (upper right) and the conservation error of the global volumetric fluid content (bottom).

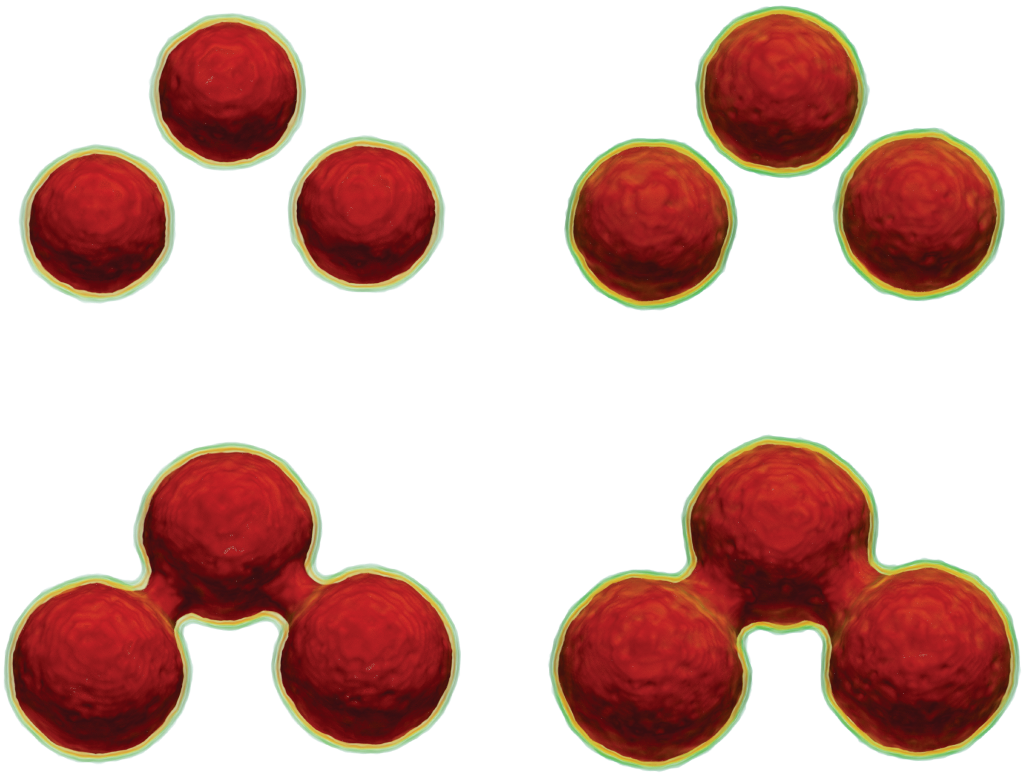

FIGURE 7 | Snapshots of the phase field ϕ at the times $t \in \{0.2, 0.5, 0.8, 1\}$ with mesh size $h_{\max} \approx 2 \cdot 10^{-2}$ and time-step $\tau = 5 \cdot 10^{-4}$. Visualisation of the tumor core ($\phi \geq 0.9$) in red and the isosurfaces $\phi = -0.25$ (green) and $\phi = 0.15$ (yellow) (from top left to bottom right).

shape. The evolution of the energy as well as the conservation error are depicted in Figure 8. In this case we have only conservation of volumetric fluid content, as well as global phase is increasing. Surprisingly, in this case we observe energy decay.

6 | Conclusion and Outlook

In this article, we proposed a structure-preserving splitting scheme for the Cahn-Hilliard-Biot system using standard finite elements in space and a problem-adapted implicit-explicit Euler time-integration method. We have shown that the method under typical assumptions has discrete solutions, which preserve the thermodynamic structure, that is, the balance of global phase, volumetric fluid content, and energy. Furthermore, under more restrictive assumptions, the uniqueness of a discrete solution is guaranteed. The theoretical results are accompanied by numerical tests, i.e., a convergence test. In addition, several test scenarios with application to tumor growth are considered and illustrated.

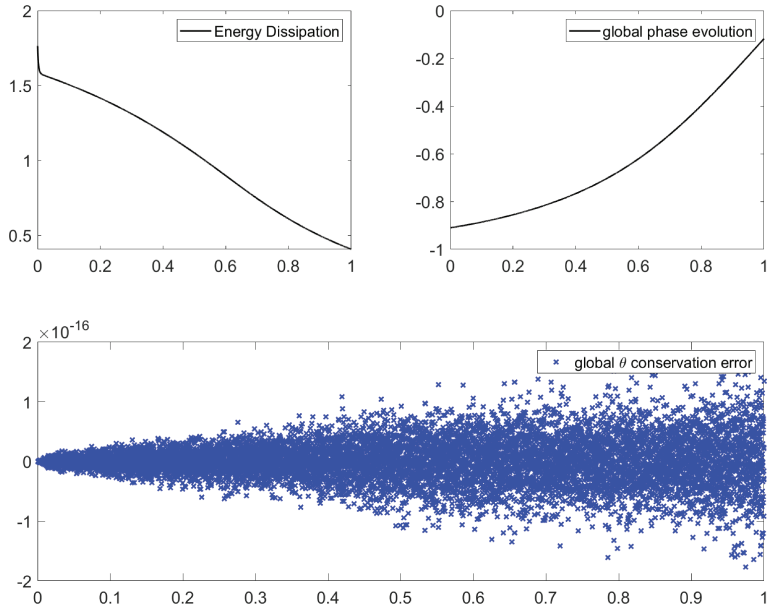

FIGURE 8 | Experiment 4: Temporal evolution of the energy dissipation (upper left) and global phase (upper right) and the global volumetric fluid content conservation error (bottom).

Acknowledgements

A.B. gratefully acknowledges the support of the German Science Foundation (DFG) via TRR 146 (project C3) and SPP2256 Project Number 441153493 and the support by the Gutenberg Research College, JGU Mainz. M.F. is supported by the State of Upper Austria. Open Access funding enabled and organized by Projekt DEAL.

Data Availability Statement

Data sharing is not applicable to this article, as no new data were created or analyzed in this study.

References

1. E. Storvik, J. W. Both, J. M. Nordbotten, and F. A. Radu, "A Cahn–Hilliard–Biot System and Its Generalized Gradient Flow Structure," *Applied Mathematics Letters* 126 (2022): 107799, https://doi.org/10.1016/j.aml.2021.107799.

2. H. Abels, H. Garcke, and J. Haselböck, "Existence of Weak Solutions to a Cahn–Hilliard–Biot System," *Nonlinear Analysis: Real World Applications* 81 (2025): 104194, https://doi.org/10.1016/j.nonrwa.2024.104194.

3. M. Milosevic, S. Lunt, E. Leung, et al., "Interstitial Permeability and Elasticity in Human Cervix Cancer," *Microvascular Research* 75, no. 3 (2008): 381–390, https://doi.org/10.1016/j.mvr.2007.11.003.

4. G. Cheng, J. Tse, R. Jain, and L. Munn, "Micro-Environmental Mechanical Stress Controls Tumor Spheroid Size and Morphology by Suppressing Proliferation and Inducing Apoptosis in Cancer Cells," *PLoS One* 4, no. 2 (2009): e4632, https://doi.org/10.1371/journal.pone.0004632.

5. G. Helmlinger, P. A. Netti, H. C. Lichtenbeld, R. J. Melder, and R. K. Jain, "Solid Stress Inhibits the Growth of Multicellular Tumor Spheroids," *Nature Biotechnology* 15, no. 8 (1997): 778–783, https://doi.org/10.1038/nbt0897-778.

6. E. Lima, J. T. Oden, D. Hormuth, T. Yankeelov, and R. Almeida, "Selection, Calibration, and Validation of Models of Tumor Growth," *Mathematical Models and Methods in Applied Sciences* 26, no. 12 (2016): 2341–2368, https://doi.org/10.1142/S021820251650055X.

7. E. Lima, J. T. Oden, B. Wohlmuth, et al., "Selection and Validation of Predictive Models of Radiation Effects on Tumor Growth Based on Noninvasive Imaging Data," *Computer Methods in Applied Mechanics and Engineering* 327 (2017): 277–305, https://doi.org/10.1016/j.cma.2017.08.009.

8. T. Stylianopoulos, J. D. Martin, V. P. Chauhan, et al., "Causes, Consequences, and Remedies for Growth-Induced Solid Stress in Murine and Human Tumors," *Proceedings of the National Academy of Sciences* 109, no. 38 (2012): 15101–15108, https://doi.org/10.1073/pnas.1213353109.

9. M. Fritz, "Tumor Evolution Models of Phase-Field Type With Nonlocal Effects and Angiogenesis," *Bulletin of Mathematical Biology* 85, no. 6 (2023): 44, https://doi.org/10.1007/s11538-023-01151-6.

10. H. Garcke, B. Kovács, and D. Trautwein, "Viscoelastic Cahn–Hilliard Models for Tumor Growth," *Mathematical Models and Methods in Applied Sciences* 32, no. 13 (2022): 2673–2758, https://doi.org/10.1142/S0218202522500634.

11. H. Garcke, K. F. Lam, and A. Signori, "On a Phase Field Model of Cahn–Hilliard Type for Tumour Growth With Mechanical Effects," *Nonlinear Analysis: Real World Applications* 57 (2021): 103192, https://doi.org/10.1016/j.nonrwa.2020.103192.

12. M. Fritz, "On the Well-Posedness of the Cahn–Hilliard–Biot Model and Its Applications to Tumor Growth," *Discrete and Continuous Dynamical Systems - Series S* 17, no. 12 (2024): 3533–3563.

13. C. Riethmüller, E. Storvik, J. W. Both, and F. A. Radu, "Well-posedness analysis of the Cahn–Hilliard–Biot model," 2023, https://doi.org/10.48550/arXiv.2310.18231, arXiv preprint arXiv:2310.18231.

14. H. Egger, "Structure Preserving Approximation of Dissipative Evolution Problems," *Numerische Mathematik* 143 (2019): 85–106, https://doi.org/10.1007/s00211-019-01050-w.

15. A. Brunk, H. Egger, and O. Habrich, "A Second-Order Structure-Preserving Discretization for the Cahn-Hilliard/Allen-Cahn System With Cross-Kinetic Coupling," *Applied Numerical Mathematics* 206 (2024a): 12–28, https://doi.org/10.1016/j.apnum, https://www.sciencedirect.com/science/article/pii/S016892742400196X.

16. A. Brunk, H. Egger, O. Habrich, and M. Lukáčová-Medvid'ová, "A second-order fully-balanced structure-preserving variational discretization scheme for the Cahn–Hilliard–Navier–Stokes system," *Mathematical Models and Methods in Applied Sciences* 33, no. 12 (2023a): 2587–2627, https://doi.org/10.1142/S0218202523500562.

17. A. Brunk, O. Habrich, T. D. Oyedeji, Y. Yang, and B.-X. Xu, "Variational Approximation for a Non-Isothermal Coupled Phase-FieldSystem: Structure-Preservation & Nonlinear Stability," *ComputationalMethods in Applied Mathematics* (2024b). Published ahead of print, https://doi.org/10.1515/cmam-2023-0274.

18. A. Brunk and D. Schumann, "Structure-preserving approximation for the non-isothermal Cahn–Hilliard–Navier–Stokes system," 2024, https://doi.org/10.48550/arXiv.2402.00147 *arXiv preprint arXiv:2402.00147*.

19. K. Shimura and S. Yoshikawa, "Error Estimate for Structure-Preserving Finite Difference Schemes of the One-Dimensional Cahn–Hilliard System Coupled With Viscoelasticity," *Regularity and Asymptotic Analysis for Critical Cases of Partial Differential Equations, Research Institute for Mathematical Sciences, Kyoto University* B82 (2020): 159–175, http://hdl.handle.net/2433/260682.

20. A. Bendimerad-Hohl, G. Haine, D. Matignon, and B. Maschke, "Structure-Preserving Discretization of a Coupled Allen–Cahn and Heat Equation System," *IFAC-PapersOnLine* 55, no. 18 (2022): 99–104, https://doi.org/10.1016/j.ifacol.2022.08.037.

21. A. Böttcher and H. Egger, "Structure Preserving Discretization of Allen–Cahn Type Problems Modeling the Motion of Phase Boundaries," *Vietnam Journal of Mathematics* 48 (2020): 847–863, https://doi.org/10.1007/s10013-020-00428-w.

22. R. Lan, J. Li, Y. Cai, and L. Ju, "Operator Splitting Based Structure-Preserving Numerical Schemes for the Mass-Conserving Convective Allen-Cahn Equation," *Journal of Computational Physics* 472 (2023): 111695, https://doi.org/10.1016/j.jcp.2022.111695.

23. H. Egger and M. Sabouri, "On the Structure Preserving High-Order Approximation of Quasistatic Poroelasticity," *Mathematics and Computers in Simulation* 189 (2021): 237–252, https://doi.org/10.1016/j.matcom.2020.12.029.

24. E. Storvik, C. Riethmüller, J. W. Both, and F. A. Radu, "Sequential Solution Strategies for the Cahn–Hilliard–Biot Model. arXiv Preprint arXiv:2401.13358," 2024, https://doi.org/10.48550/arXiv.2401.13358.

25. J. Barrett, H. Garcke, and R. Nürnberg, "Finite Element Approximation of a Phase Field Model for Surface Diffusion of Voids in a Stressed Solid," *Mathematics of Computation* 75, no. 253 (2006): 7–41, https://doi.org/10.1090/S0025-5718-05-01802-8.

26. T. Blesgen and I. V. Chenchiah, "Cahn–Hilliard Equations Incorporating Elasticity: Analysis and Comparison to Experiments," *Philosophical Transactions of the Royal Society A: Mathematical, Physical and Engineering Sciences* 371, no. 2005 (2013): 20120342, https://doi.org/10.1098/rsta.2012.0342.

27. K. Shimura and S. Yoshikawa, "A New Conservative Finite Difference Scheme for 1d Cahn–Hilliard Equation Coupled With Elasticity," *Journal of Applied Analysis* 28, no. 2 (2022): 311–332, https://doi.org/10.1515/jaa-2021-2071.

28. C. Gräser, R. Kornhuber, and U. Sack, "Numerical Simulation of Coarsening in Binary Solder Alloys," *Computational Materials Science* 93 (2014): 221–233, https://doi.org/10.1016/j.commatsci.2014.06.010.

29. H. Garcke, R. Nürnberg, and V. Styles, "Stress-and Diffusion-Induced Interface Motion: Modelling and Numerical Simulations," *European Journal of Applied Mathematics* 18, no. 6 (2007): 631–657, https://doi.org/10.1017/S095679250700719X.

30. H. Garcke and U. Weikard, "Numerical Approximation of the Cahn–Larché Equation," *Numerische Mathematik* 100, no. 4 (2005): 639–662, https://doi.org/10.1007/s00211-004-0578-x.

31. L. Dedè, M. J. Borden, and T. J. Hughes, "Isogeometric Analysis for Topology Optimization With a Phase Field Model," *Archives of Computational Methods in Engineering* 19 (2012): 427–465, https://doi.org/10.1007/s11831-012-9075-z.

32. S. Bartels and R. Müller, "A Posteriori Error Controlled Local Resolution of Evolving Interfaces for Generalized Cahn–Hilliard Equations," *Interfaces and Free Boundaries* 12, no. 1 (2010): 45–74, https://doi.org/10.4171/ifb/226.

33. E. Storvik, J. W. Both, J. M. Nordbotten, and F. A. Radu, "A Robust Solution Strategy for the Cahn-Larché Equations," *Computers & Mathematics with Applications* 136 (2023): 112–126, https://doi.org/10.1016/j.camwa.2023.02.002, https://www.sciencedirect.com/science/article/pii/S0898122123000536.

34. P. Areias, E. Samaniego, and T. Rabczuk, "A Staggered Approach for the Coupling of Cahn–Hilliard Type Diffusion and Finite Strain Elasticity," *Computational Mechanics* 57, no. 2 (2015): 339–351, https://doi.org/10.1007/s00466-015-1235-1.

35. J. Wloka, "*Partial Differential Equations*," (Cambridge: Cambridge University Press, 1987), https://doi.org/10.1017/CBO9781139171755.

36. A. Brunk, H. Egger, O. Habrich, and M. Lukáčová-Medvid'ová, "Stability and Discretization Error Analysis for the Cahn–Hilliard System Via Relative Energy Estimates," *ESAIM. Mathematical Modelling and Numerical Analysis* 57, no. 3 (2023b): 1297–1322, https://doi.org/10.1051/m2an/2023017.

37. H. Garcke and D. Trautwein, "Numerical Analysis for a Cahn–Hilliard System Modelling Tumour Growth With Chemotaxis and Active Transport," *Journal of Numerical Mathematics* 30, no. 4 (2022): 295–324, https://doi.org/10.1515/jnma-2021-0094.

38. S. Bartels, "*Numerical Methods for Nonlinear Partial Differential Equations*," (New York: Springer: 2015).

39. E. Zeidler, *Nonlinear Functional Analysis and Its Applications I: Fixed-Point Theorems* (New York: Springer, 1986).

40. J. W. Barrett, J. F. Blowey, and H. Garcke, "Finite Element Approximation of the Cahn–Hilliard Equation With Degenerate Mobility," *SIAM Journal on Numerical Analysis* 37, no. 1 (1999): 286–318, https://doi.org/10.1137/S0036142997331669.

41. S. C. Brenner and L. R. Scott, *The Mathematical Theory of Finite Element Methods* (New York: Springer, 2008), https://doi.org/10.1007/978-0-387-75934-0.

42. J. Schöberl, "*C* + +11 Implementation of Finite Elements in Ngsolve," *Institute for Analysis and Scientific Computing, Vienna University of Technology* 30 (2014): 1–23, http://hdl.handle.net/20.500.12708/28346.

43. D. J. Eyre, "Unconditionally Gradient Stable Time Marching the Cahn-Hilliard Equation," *Materials Research Society Symposium Proceedings* 529 (1998): 39–46, https://doi.org/10.1557/PROC-529-39.